Microphone array beamforming based on maximization of the front-to-back ratio

Xianghui Wang,[1,a)] Jacob Benesty,[2] Israel Cohen,[3] and Jingdong Chen[1,b)]
[1]*Center of Intelligent Acoustics and Immersive Communications and School of Marine Science and Technology, Northwestern Polytechnical University, 127 Youyi West Road, Xi'an 710072, China*
[2]*Institut National de la Recherche Scientifique, Centre Énergie Matériaux Télécommunications, University of Quebec, 800 de la Gauchetiere Ouest, Montreal, Quebec H5A 1K6, Canada*
[3]*Andrew and Erna Viterby Faculty of Electrical Engineering, Technion-Israel Institute of Technology, Technion City, Haifa 32000, Israel*

(Received 29 May 2018; revised 13 November 2018; accepted 16 November 2018; published online 21 December 2018)

Microphone arrays are typically used in room acoustic environments to acquire high fidelity audio and speech signals while suppressing noise, interference, and reverberation. In many application scenarios, interference and reverberation may mainly come from a certain region, and it is therefore necessary to develop beamformers that can preserve signals of interest while minimizing the power of signals coming from the region where interference and reverberation dominate. For this purpose, this paper first reexamines the so-called front-to-back ratio and the classical supercardioid beamformer. To deal with the white noise amplification problem and the limited directivity factor associated with the supercardioid beamformer, a set of reduced-rank beamformers are deduced by using the well-known joint diagonalization technique, which can make compromises between the front-to-back ratio and the amount of white noise amplification or the directivity factor. Then, the definition of the front-to-back ratio is extended to a generalized version, from which another set of reduced-rank beamformers and their regularized versions are developed. Simulations are conducted to illustrate the properties and advantages of the proposed beamformers.
 https://doi.org/10.1121/1.5082548

[NX] Pages: 3450–3464

I. INTRODUCTION

Beamforming with microphone arrays has attracted much attention recently due to its wide range of applications, such as hands-free voice communications and human-machine interfaces (Brandstein and Ward, 2001; Benesty *et al.*, 2008; Benesty *et al.*, 2017). Many beamforming algorithms were developed in the literature such as the delay-and-sum (DS) beamformer (Schelkunoff, 1943), broadband beamformers based narrowband decomposition (Doclo and Moonen, 2003; Benesty *et al.*, 2007; Capon, 1969; Frost, 1972) and nested arrays (Zheng *et al.*, 2004; Kellermann, 1991; Elko and Meyer, 2008), modal beamformers (Torres *et al.*, 2012; Yan *et al.*, 2011; Koyama *et al.*, 2016; Park and Rafaely, 2005), superdirective beamformers (Cox *et al.*, 1986; Kates, 1993; Wang *et al.*, 2014), and differential beamformers with differential microphone arrays (DMAs) (Elko, 2000; Elko and Meyer, 2008; Chen *et al.*, 2014; Pan *et al.*, 2015b; Abhayapala and Gupta, 2010; Weinberger *et al.*, 1933; Olson, 1946; Sessler and West, 1971; Warren and Thompson, 2006). Among these, differential beamformers are now widely used in a wide spectrum of small devices such as smart speakers, smartphones, and robotics, primarily because they exhibit frequency-invariant beampatterns and can achieve high directivity factors (DFs) with small apertures.

The basic principle of DMAs can be traced back to the 1930s when directional ribbon microphones were developed (Weinberger *et al.*, 1933; Olson, 1946). Since then, much effort has been devoted to the design and study of DMAs from different perspectives. For example, the cascaded method was investigated to design different orders of DMAs with different beampatterns (such as the cardioid, dipole, supercardioid, hypercardioid, etc.) (Elko, 2000; Elko and Meyer, 2008; Abhayapala and Gupta, 2010). Theoretical analysis of the principle of the DMA by gradient analysis were carried out in Kolundžija *et al.* (2011). The performance of the first-order DMAs was investigated under sensor imperfection in Buck (2002). The DF and the model for deviation of the DMAs were analyzed in the frequency domain in Buck and Rößler (2001). Adaptive first- and second-order DMAs were proposed in Teutsch and Elko (2001) for attenuating interference moving in the rear-half plane of the array, which was then analyzed in Elko and Meyer (2009) and Elko *et al.* (1996) also. Several kinds of steerable DMAs were developed and analyzed in Elko and Pong (1997), Derkx and Janse (2009), and Huang *et al.* (2017). In Ihle (2003), Benesty *et al.* (2012), and Song and Liu (2008), DMAs were studied from the perspectives of power spectral density estimation and noise reduction, respectively. Different ways of designing higher-order DMAs are presented in Sena *et al.* (2012) and Abhayapala and Gupta (2010). Recently, a so-called null-constrained method was developed in the frequency domain (Benesty and Chen, 2012; Benesty *et al.*, 2015; Chen *et al.*, 2014),

[a)]Also at: Andrew and Erna Viterby Faculty of Electrical Engineering, Technion-Israel Institute of Technology, Technion City, Haifa 32000, Israel.
[b)]Electronic mail: jingdongchen@ieee.org

which enables the design of DMAs by using the distortionless and null constraints. With this method, a minimum-norm solution can be derived to improve the white noise gain (WNG) by exploiting the redundancy provided by using more microphones, thereby circumventing the problem of white noise amplification (Benesty and Chen, 2012; Chen *et al.*, 2014). A series expansion based approach to DMA design is presented in Zhao *et al.* (2014) and Pan *et al.* (2015a). Now, DMAs have been widely used in a wide range of applications such as hearing aids Slavin (1987), smart-speakers, bluetooth headphones, in-car navigation systems, etc.

The DF and WNG are two popular performance measures used for designing and evaluating differential beamformers. These two measures, however, do not take into account source and interference distribution information. In many typical application scenarios, the source of interest may be confined in one region while interference sources and strong reflection paths are distributed in another region. For example, a television is placed against a wall and a microphone array is placed in front of a TV. In this case, the source of interest is incident from the front half of the plane while interference from TV loudspeakers is from the back half of the plane. In such situations, it is desirable to design beamformers that can preserve signals of interest while minimizing the power of signals coming from the region where interference and reverberation dominate. For this purpose, we revisit the definition of the so-called front-to-back ratio (FBR) and present a generalized FBR (GFBR), based on which a number of differential beamformers are deduced. The major contributions are as follows. (1) From the FBR, the classical supercardioid beamformer is deduced, which achieves maximum FBR with almost frequency-invariant beampattern. But this beamformer suffers from the problem of white noise amplification, which is particularly serious at low frequencies, and its DF is limited also. (2) To overcome the drawbacks of the supercardioid beamformer, a set of reduced-rank beamformers and their regularized version are developed from the WNG and DF maximization perspectives, respectively, using the well-known joint diagonalization technique. These beamformers can compromise between the FBR and WNG or DF flexibly by adjusting the algorithmic parameters. (3) The definition of the FBR is extended to GFBR. (4) Based on GFBR, another set of reduced-rank beamformers and its regularized version are developed. Simulations are conducted to illustrate the properties and advantages of the proposed beamformers.

The remainder of the paper is organized as follows. The signal model and problem formulation are presented in Sec. II. Section III defines some useful performance measures and introduces some traditional fixed beamformers. The joint diagonalization is briefly described in Sec. IV. Section V deduces the supercardioid beamformer, two kinds of reduced-rank beamformers, and one regularized version. The FBR is generalized to GFBR, and two other reduced-rank beamformers and another regularized version are developed in Sec. VI. Simulations are conducted in Sec. VII and conclusions are drawn in Sec. VIII.

II. SIGNAL MODEL AND PROBLEM FORMULATION

We consider a farfield plane wave that propagates in an anechoic acoustic environment at the speed of sound, i.e., $c = 340$ m/s, and impinges on a uniform linear sensor array consisting of M omnidirectional microphones, where the inter-element spacing is equal to δ. Denote by θ the incidence angle. In this context, the steering vector of length M is given by

$$\mathbf{d}(\omega,\theta) = [1 \;\; e^{-\jmath\omega\tau_0\cos\theta} \;\; \cdots \;\; e^{-\jmath(M-1)\omega\tau_0\cos\theta}]^T, \tag{1}$$

where the superscript ^{T} is the transpose operator, $\jmath = \sqrt{-1}$ is the imaginary unit, $\omega = 2\pi f$ is the angular frequency, $f > 0$ is the temporal frequency, and $\tau_0 = \delta/c$ is the time delay between two successive sensors at the angle $\theta = 0$.

In this study, we consider fixed directional beamformers with small values of δ, like in differential (Elko and Meyer, 2008; Elko, 2000; Benesty and Chen, 2012) or superdirective (Cox *et al.*, 1986; Cox *et al.*, 1987) beamforming, where the main lobe is at the angle $\theta = 0$ (endfire direction) and it is assumed that the desired signal propagates also from this angle. Since the source is assumed to propagate from the angle $\theta = 0$, the signals observed by the microphone array are given by

$$\begin{aligned}\mathbf{y}(\omega) &= [Y_1(\omega)\, Y_2(\omega) \cdots Y_M(\omega)]^T \\ &= \mathbf{x}(\omega) + \mathbf{v}(\omega) \\ &= \mathbf{d}(\omega,0)X(\omega) + \mathbf{v}(\omega),\end{aligned} \tag{2}$$

where $Y_m(\omega)$ is the mth microphone signal, $\mathbf{x}(\omega) = \mathbf{d}(\omega,0)X(\omega)$, $X(\omega)$ is the zero-mean desired signal, $\mathbf{d}(\omega,0)$ is the signal propagation vector (also steering vector at $\theta = 0$), and $\mathbf{v}(\omega)$ is the zero-mean additive noise signal vector, which is defined similarly to $\mathbf{y}(\omega)$. The desired signal and additive noise are assumed to be uncorrelated with each other. The beamformer output is then (Benesty *et al.*, 2008)

$$\begin{aligned}Z(\omega) &= \mathbf{h}^H(\omega)\mathbf{y}(\omega) \\ &= \mathbf{h}^H(\omega)\mathbf{d}(\omega,0)X(\omega) + \mathbf{h}^H(\omega)\mathbf{v}(\omega),\end{aligned} \tag{3}$$

where $Z(\omega)$ is the estimate of the desired signal, $X(\omega)$,

$$\mathbf{h}(\omega) = [H_1(\omega)\, H_2(\omega) \cdots H_M(\omega)]^T \tag{4}$$

is a complex-valued linear filter applied to the observation signal vector, $\mathbf{y}(\omega)$, and the superscripts * and ^{H} denote complex-conjugate and conjugate-transpose, respectively. In our context, the distortionless constraint is desired, i.e.,

$$\mathbf{h}^H(\omega)\mathbf{d}(\omega,0) = 1. \tag{5}$$

Then, the objective of this work is to design beamformers, i.e., to find optimal beamforming filters, $\mathbf{h}(\omega)$, with a uniform linear array (ULA) based on the maximization of the FBR or its generalized version subject to the constraint given in Eq. (5).

III. PERFORMANCE MEASURES

Before discussing how to design different beamformers, let us first present a few performance measures, which have

been intensively investigated in the literature and are efficient for evaluating the performance of beamformers.

The first important measure, which describes the sensitivity of the beamformer to a plane wave impinging on the array from the direction θ, is the beampattern. It is given by

$$\begin{aligned}\mathcal{B}[\mathbf{h}(\omega),\theta] &= \mathbf{d}^H(\omega,\theta)\mathbf{h}(\omega)\\ &= \sum_{m=1}^{M} H_m(\omega)e^{\jmath(m-1)\omega\tau_0\cos\theta}.\end{aligned} \tag{6}$$

Plotting the magnitude of $\mathcal{B}[\mathbf{h}(\omega),\theta]$ as a function of θ gives us much information about the performance of the beamformer, $\mathbf{h}(\omega)$, including the beamwidth (the range between the first nulls on each side of the main lobe), the sidelobe level, etc. Generally, the narrower the beamwidth and the lower the sidelobe level, the better is the performance of the beamformer. Also, plotting the magnitude of $\mathcal{B}[\mathbf{h}(\omega),\theta]$ with respect to ω indicates how well the beamformer preserves the fidelity of a wideband signal.

Some beamformers are sensitive to the array imperfections, such as microphones' self-noise, nonuniform responses among the microphones, imprecisions of the microphone positions, etc. One way to evaluate this is through the so-called WNG, which is defined as

$$\mathcal{W}[\mathbf{h}(\omega)] = \frac{|\mathbf{h}^H(\omega)\mathbf{d}(\omega,0)|^2}{\mathbf{h}^H(\omega)\mathbf{h}(\omega)}. \tag{7}$$

It should be noted that $\mathcal{W}[\mathbf{h}(\omega)] < 1$ means that the white noise is amplified. It can be verified that this gain is maximized with the classical DS beamformer

$$\mathbf{h}_{\mathrm{DS}}(\omega) = \frac{\mathbf{d}(\omega,0)}{M}, \tag{8}$$

and the maximum WNG is given by

$$\mathcal{W}_{\max} = \mathcal{W}[\mathbf{h}_{\mathrm{DS}}(\omega)] = M, \tag{9}$$

which is frequency independent.

Another important measure, which quantifies how the microphone array performs in the spherically isotropic (diffuse) noise field is the DF, which is defined as

$$\begin{aligned}\mathcal{D}[\mathbf{h}(\omega)] &= \frac{|\mathcal{B}[\mathbf{h}(\omega),0]|^2}{\frac{1}{2}\int_0^{\pi}|\mathcal{B}[\mathbf{h}(\omega),\theta]|^2\sin\theta d\theta}\\ &= \frac{|\mathbf{h}^H(\omega)\mathbf{d}(\omega,0)|^2}{\mathbf{h}^H(\omega)\Gamma_{0,\pi}(\omega)\mathbf{h}(\omega)},\end{aligned} \tag{10}$$

where

$$\mathbf{\Gamma}_{0,\pi}(\omega) = \frac{1}{2}\int_0^{\pi}\mathbf{d}(\omega,\theta)\mathbf{d}^H(\omega,\theta)\sin\theta d\theta. \tag{11}$$

Actually, in the spherically isotropic noise field, a more general definition is

$$\mathbf{\Gamma}_{\psi_1,\psi_2}(\omega) = \mathcal{N}_{\psi_1,\psi_2}\int_{\psi_1}^{\psi_2}\mathbf{d}(\omega,\theta)\mathbf{d}^H(\omega,\theta)\sin\theta d\theta, \tag{12}$$

where

$$\mathcal{N}_{\psi_1,\psi_2} = \frac{1}{\int_{\psi_1}^{\psi_2}\sin\theta d\theta} = \frac{1}{\cos\psi_1-\cos\psi_2}. \tag{13}$$

It can easily be verified that

$$\begin{aligned}\left[\mathbf{\Gamma}_{\psi_1,\psi_2}(\omega)\right]_{ij} &= \mathcal{N}_{\psi_1,\psi_2}\\ &\times\frac{e^{\jmath\omega(j-i)\tau_0\cos\psi_1}-e^{\jmath\omega(j-i)\tau_0\cos\psi_2}}{\jmath\omega(j-i)\tau_0},\end{aligned} \tag{14}$$

with $[\mathbf{\Gamma}_{\psi_1,\psi_2}(\omega)]_{mm} = 1$, $m = 1,2,\ldots,M$. Accordingly, the elements of the $M\times M$ matrix $\mathbf{\Gamma}_{0,\pi}(\omega)$ are (Benesty and Chen, 2012)

$$\begin{aligned}\left[\mathbf{\Gamma}_{0,\pi}(\omega)\right]_{ij} &= \frac{\sin[\omega(j-i)\tau_0]}{\omega(j-i)\tau_0}\\ &= \mathrm{sinc}[\omega(j-i)\tau_0],\end{aligned} \tag{15}$$

with $[\mathbf{\Gamma}_{0,\pi}(\omega)]_{mm} = 1$, $m = 1,2,\ldots,M$. One can check that the DF is maximized with the classical superdirective beamformer (which coincides with the hypercardioid beamformer of order $M-1$) (Cox *et al.*, 1986; Cox *et al.*, 1987),

$$\mathbf{h}_{\mathrm{S}}(\omega) = \frac{\mathbf{\Gamma}_{0,\pi}^{-1}(\omega)\mathbf{d}(\omega,0)}{\mathbf{d}^H(\omega,0)\mathbf{\Gamma}_{0,\pi}^{-1}(\omega)\mathbf{d}(\omega,0)} \tag{16}$$

and the maximum DF is given by

$$\begin{aligned}\mathcal{D}_{\max}(\omega) &= \mathcal{D}[\mathbf{h}_{\mathrm{S}}(\omega)]\\ &= \mathbf{d}^H(\omega,0)\mathbf{\Gamma}_{0,\pi}^{-1}(\omega)\mathbf{d}(\omega,0),\end{aligned} \tag{17}$$

which is frequency dependent. It can be shown that (Uzkov, 1946)

$$\lim_{\delta\to 0}\mathcal{D}_{\max}(\omega) = M^2,\ \forall\omega, \tag{18}$$

which is referred as the supergain in the literature. This gain can be achieved but at the expense of white noise amplification.

The last measure that we discuss in this section is the FBR, which is defined as the ratio of the power of the output of the array to signals propagating from the front-half plane to the output power for signals arriving from the rear-half plane (Marshall and Harry, 1941). This ratio, for the spherically isotropic noise field, is mathematically defined as (Marshall and Harry, 1941)

$$\begin{aligned}\mathcal{F}[\mathbf{h}(\omega)] &= \frac{\int_0^{\pi/2}|\mathcal{B}[\mathbf{h}(\omega),\theta]|^2\sin\theta d\theta}{\int_{\pi/2}^{\pi}|\mathcal{B}[\mathbf{h}(\omega),\theta]|^2\sin\theta d\theta}\\ &= \frac{\mathbf{h}^H(\omega)\mathbf{\Gamma}_{0,\pi/2}(\omega)\mathbf{h}(\omega)}{\mathbf{h}^H(\omega)\mathbf{\Gamma}_{\pi/2,\pi}(\omega)\mathbf{h}(\omega)},\end{aligned} \tag{19}$$

where

$$\left[\mathbf{\Gamma}_{0,\pi/2}(\omega)\right]_{ij} = \frac{e^{\jmath\omega(j-i)\tau_0} - 1}{\jmath\omega(j-i)\tau_0} \tag{20}$$

and

$$\left[\mathbf{\Gamma}_{\pi/2,\pi}(\omega)\right]_{ij} = \frac{1 - e^{-\jmath\omega(j-i)\tau_0}}{\jmath\omega(j-i)\tau_0}, \tag{21}$$

with $[\mathbf{\Gamma}_{0,\pi/2}(\omega)]_{mm} = [\mathbf{\Gamma}_{\pi/2,\pi}(\omega)]_{mm} = 1$, $m = 1, 2, \ldots, M$ according to Eq. (14). The FBR measure was studied in the existing literature, but only for designing the supercardioid beamformer.

We conclude this section with an obvious relationship between the DF and FBR. Indeed, we can write the DF as

$$\begin{aligned}\mathcal{D}[\mathbf{h}(\omega)] &= \frac{2|\mathbf{h}^H(\omega)\mathbf{d}(\omega,0)|^2}{\mathbf{h}^H(\omega)\left[\mathbf{\Gamma}_{0,\pi/2}(\omega) + \mathbf{\Gamma}_{\pi/2,\pi}(\omega)\right]\mathbf{h}(\omega)} \\ &= \frac{2\mathcal{D}'[\mathbf{h}(\omega)]}{1 + \mathcal{F}[\mathbf{h}(\omega)]},\end{aligned} \tag{22}$$

where

$$\mathcal{D}'[\mathbf{h}(\omega)] = \frac{|\mathbf{h}^H(\omega)\mathbf{d}(\omega,0)|^2}{\mathbf{h}^H(\omega)\mathbf{\Gamma}_{\pi/2,\pi}(\omega)\mathbf{h}(\omega)}. \tag{23}$$

We see that maximizing $\mathcal{D}'[\mathbf{h}(\omega)]$ is equivalent to minimizing the energy of the diffuse noise at the back of the beampattern subject to the distortionless constraint. Therefore, $\mathcal{D}'[\mathbf{h}(\omega)]$ can also be a very useful measure.

IV. JOINT DIAGONALIZATION

Joint diagonalization is a useful tool to derive different kinds of compromising beamformers or filters.

Let us assume that $\mathbf{\Gamma}_{\pi/2,\pi}(\omega)$ is a full-rank matrix, which should be true in principle. Then, the two Hermitian matrices $\mathbf{\Gamma}_{0,\pi/2}(\omega)$ and $\mathbf{\Gamma}_{\pi/2,\pi}(\omega)$ can be, indeed, jointly diagonalized as follows (Franklin, 1968):

$$\mathbf{T}^H(\omega)\mathbf{\Gamma}_{0,\pi/2}(\omega)\mathbf{T}(\omega) = \mathbf{\Lambda}(\omega), \tag{24}$$

$$\mathbf{T}^H(\omega)\mathbf{\Gamma}_{\pi/2,\pi}(\omega)\mathbf{T}(\omega) = \mathbf{I}_M, \tag{25}$$

where

$$\mathbf{T}(\omega) = [\,\mathbf{t}_1(\omega)\,\mathbf{t}_2(\omega)\,\cdots\,\mathbf{t}_M(\omega)\,] \tag{26}$$

is a full-rank square matrix (of size $M \times M$), but not necessarily orthogonal, and

$$\mathbf{\Lambda}(\omega) = \mathrm{diag}[\,\lambda_1(\omega), \lambda_2(\omega), \ldots, \lambda_M(\omega)\,] \tag{27}$$

is a diagonal matrix whose main elements are real and nonnegative. Furthermore, $\mathbf{\Lambda}(\omega)$ and $\mathbf{T}(\omega)$ are the eigenvalue and eigenvector matrices, respectively, of $\mathbf{\Gamma}^{-1}_{\pi/2,\pi}(\omega)\mathbf{\Gamma}_{0,\pi/2}(\omega)$, i.e.,

$$\mathbf{\Gamma}^{-1}_{\pi/2,\pi}(\omega)\mathbf{\Gamma}_{0,\pi/2}(\omega)\mathbf{T}(\omega) = \mathbf{T}(\omega)\mathbf{\Lambda}(\omega). \tag{28}$$

It is assumed that the eigenvalues of $\mathbf{\Gamma}^{-1}_{\pi/2,\pi}(\omega)\mathbf{\Gamma}_{0,\pi/2}(\omega)$ are ordered as $\lambda_1(\omega) \geq \lambda_2(\omega) \geq \cdots \geq \lambda_M(\omega) \geq 0$. Therefore, the corresponding eigenvectors are $\mathbf{t}_1(\omega), \mathbf{t}_2(\omega), \ldots, \mathbf{t}_M(\omega)$.

V. BEAMFORMERS FROM AN FBR MAXIMIZATION PERSPECTIVE

In this section, we discuss several differential beamformers, which are derived directly from the FBR in tandem with joint diagonalization of the Hermitian matrices that are contained in this measure.

A. Maximum FBR

In Eq. (19), we recognize the generalized Rayleigh quotient (Golub and Loan, 1996). It is well known that this quotient is maximized with the eigenvector corresponding to the maximum eigenvalue of $\mathbf{\Gamma}^{-1}_{\pi/2,\pi}(\omega)\mathbf{\Gamma}_{0,\pi/2}(\omega)$. Therefore, the maximum FBR beamformer is

$$\mathbf{h}_{\mathrm{mFBR}}(\omega) = \alpha(\omega)\mathbf{t}_1(\omega), \tag{29}$$

where $\alpha(\omega) \neq 0$ is an arbitrary complex number. We deduce that

$$\mathcal{F}[\mathbf{h}_{\mathrm{mFBR}}(\omega)] = \lambda_1(\omega). \tag{30}$$

Clearly, we always have

$$\mathcal{F}[\mathbf{h}_{\mathrm{mFBR}}(\omega)] \geq \mathcal{F}[\mathbf{h}(\omega)],\ \forall \mathbf{h}(\omega). \tag{31}$$

B. Supercardioid

In practice, it is important to properly choose the value of $\alpha(\omega)$. The most obvious thing to do is to find this parameter in such a way that the maximum FBR beamformer is distortionless. Substituting Eq. (29) in Eq. (5), we get

$$\alpha(\omega) = \frac{1}{\mathbf{d}^H(\omega,0)\mathbf{t}_1(\omega)}. \tag{32}$$

Substituting Eq. (32) in Eq. (29), we obtain the supercardioid beamformer of order $M-1$,

$$\mathbf{h}_{\mathrm{SC}}(\omega) = \frac{\mathbf{t}_1(\omega)}{\mathbf{d}^H(\omega,0)\mathbf{t}_1(\omega)}. \tag{33}$$

C. Reduced rank

In this subsection, we consider beamformers that have the form

$$\mathbf{h}_Q(\omega) = \mathbf{T}_{1:Q}(\omega)\mathbf{g}_{1:Q}(\omega), \tag{34}$$

where

$$\mathbf{T}_{1:Q}(\omega) = \left[\,\mathbf{t}_1(\omega)\,\mathbf{t}_2(\omega)\,\cdots\,\mathbf{t}_Q(\omega)\,\right] \tag{35}$$

is a matrix of size $M \times Q$, with $1 \leq Q \leq M$, and

$$\mathbf{g}_{1:Q}(\omega) = \left[\,G_1(\omega)\,G_2(\omega)\,\cdots\,G_Q(\omega)\,\right]^T \neq \mathbf{0} \tag{36}$$

is a vector of length Q. In this case, we can express FBR as

$$\mathcal{F}\left[\mathbf{h}_Q(\omega)\right] = \frac{\mathbf{h}_Q^H(\omega)\mathbf{\Gamma}_{0,\pi/2}(\omega)\mathbf{h}_Q(\omega)}{\mathbf{h}_Q^H(\omega)\mathbf{\Gamma}_{\pi/2,\pi}(\omega)\mathbf{h}_Q(\omega)} = \frac{\mathbf{g}_{1:Q}^H(\omega)\mathbf{\Lambda}_{1:Q}(\omega)\mathbf{g}_{1:Q}(\omega)}{\mathbf{g}_{1:Q}^H(\omega)\mathbf{g}_{1:Q}(\omega)} = \mathcal{F}\left[\mathbf{g}_{1:Q}(\omega)\right], \tag{37}$$

where

$$\mathbf{\Lambda}_{1:Q}(\omega) = \text{diag}\left[\,\lambda_1(\omega), \lambda_2(\omega), \ldots, \lambda_Q(\omega)\,\right]. \tag{38}$$

It can be shown that

$$\mathcal{F}\left[\mathbf{g}_{1:1}(\omega)\right] \geq \mathcal{F}\left[\mathbf{g}_{1:2}(\omega)\right] \geq \cdots \geq \mathcal{F}\left[\mathbf{g}_{1:M}(\omega)\right]. \tag{39}$$

With the filter given in Eq. (34), we can also write the WNG as

$$\mathcal{W}\left[\mathbf{h}_Q(\omega)\right] = \frac{|\mathbf{h}_Q^H(\omega)\mathbf{d}(\omega,0)|^2}{\mathbf{h}_Q^H(\omega)\mathbf{h}_Q(\omega)} = \frac{|\mathbf{g}_{1:Q}^H(\omega)\mathbf{T}_{1:Q}^H(\omega)\mathbf{d}(\omega,0)|^2}{\mathbf{g}_{1:Q}^H(\omega)\mathbf{T}_{1:Q}^H(\omega)\mathbf{T}_{1:Q}(\omega)\mathbf{g}_{1:Q}(\omega)} = \mathcal{W}\left[\mathbf{g}_{1:Q}(\omega)\right]. \tag{40}$$

Now, our goal is to maximize Eq. (40). This is equivalent to

$$\begin{aligned} &\min_{\mathbf{g}_{1:Q}(\omega)} \mathbf{g}_{1:Q}^H(\omega)\mathbf{T}_{1:Q}^H(\omega)\mathbf{T}_{1:Q}(\omega)\mathbf{g}_{1:Q}(\omega) \\ &\text{subject to } \mathbf{g}_{1:Q}^H(\omega)\mathbf{T}_{1:Q}^H(\omega)\mathbf{d}(\omega,0) = 1, \end{aligned} \tag{41}$$

whose solution is

$$\mathbf{g}_{1:Q}(\omega) = \frac{\left[\mathbf{T}_{1:Q}^H(\omega)\mathbf{T}_{1:Q}(\omega)\right]^{-1}\mathbf{T}_{1:Q}^H(\omega)\mathbf{d}(\omega,0)}{\mathbf{d}^H(\omega,0)\mathbf{P}_{1,1:Q}(\omega)\mathbf{d}(\omega,0)}, \tag{42}$$

where

$$\mathbf{P}_{1,1:Q}(\omega) = \mathbf{T}_{1:Q}(\omega)\left[\mathbf{T}_{1:Q}^H(\omega)\mathbf{T}_{1:Q}(\omega)\right]^{-1}\mathbf{T}_{1:Q}^H(\omega) \tag{43}$$

is a projection matrix of rank Q. As a result, the reduced-rank beamformer is

$$\mathbf{h}_{Q,\text{RR}}(\omega) = \frac{\mathbf{P}_{1,1:Q}(\omega)\mathbf{d}(\omega,0)}{\mathbf{d}^H(\omega,0)\mathbf{P}_{1,1:Q}(\omega)\mathbf{d}(\omega,0)}. \tag{44}$$

For $Q=1$, we get

$$\mathbf{h}_{1,\text{RR}}(\omega) = \mathbf{h}_{\text{SC}}(\omega), \tag{45}$$

which is the supercardioid beamformer, and for $Q=M$, we obtain

$$\mathbf{h}_{M,\text{RR}}(\omega) = \frac{\mathbf{d}(\omega,0)}{\mathbf{d}^H(\omega,0)\mathbf{d}(\omega,0)}, \tag{46}$$

which corresponds to the DS beamformer obtained from the maximization of $\mathcal{W}[\mathbf{h}(\omega)]$ defined in Eq. (7).

We can also exploit the joint diagonalization in the definition of the DF in Eq. (22), which can be expressed with $\mathbf{h}_Q(\omega)$ as

$$\mathcal{D}\left[\mathbf{h}_Q(\omega)\right] = \frac{2|\mathbf{g}_{1:Q}^H(\omega)\mathbf{T}_{1:Q}^H(\omega)\mathbf{d}(\omega,0)|^2}{\mathbf{g}_{1:Q}^H(\omega)\left[\mathbf{\Lambda}_{1:Q}(\omega)+\mathbf{I}_Q\right]\mathbf{g}_{1:Q}(\omega)} = \mathcal{D}\left[\mathbf{g}_Q(\omega)\right], \tag{47}$$

where $\mathbf{I}_Q$ is the $Q\times Q$ identity matrix. Maximizing Eq. (47) is equivalent to

$$\begin{aligned} &\min_{\mathbf{g}_{1:Q}(\omega)} \mathbf{g}_{1:Q}^H(\omega)\left[\mathbf{\Lambda}_{1:Q}(\omega)+\mathbf{I}_Q\right]\mathbf{g}_{1:Q}(\omega) \\ &\text{subject to } \mathbf{g}_{1:Q}^H(\omega)\mathbf{T}_{1:Q}^H(\omega)\mathbf{d}(\omega,0) = 1, \end{aligned} \tag{48}$$

from which it is not difficult to find our second reduced-rank beamformer

$$\mathbf{h}_{Q,\text{RR2}}(\omega) = \frac{\mathbf{P}_{2,1:Q}(\omega)\mathbf{d}(\omega,0)}{\mathbf{d}^H(\omega,0)\mathbf{P}_{2,1:Q}(\omega)\mathbf{d}(\omega,0)}, \tag{49}$$

where

$$\mathbf{P}_{2,1:Q}(\omega) = \mathbf{T}_{1:Q}(\omega)\left[\mathbf{\Lambda}_{1:Q}(\omega)+\mathbf{I}_Q\right]^{-1}\mathbf{T}_{1:Q}^H(\omega). \tag{50}$$

Now, for $Q=1$, we get the supercardioid beamformer, i.e., $\mathbf{h}_{1,\text{RR2}}(\omega) = \mathbf{h}_{\text{SC}}(\omega)$, and for $Q=M$, we get the superdirective (hypercardioid) beamformer, i.e., $\mathbf{h}_{M,\text{RR2}}(\omega) = \mathbf{h}_{\text{S}}(\omega)$. Therefore, with this approach, we can obtain interesting beamformers with performance between those of the supercardioid and the hypercardioid beamformers. It can be verified that (see the Appendix)

$$\mathcal{F}\left[\mathbf{h}_{1,\text{RR2}}(\omega)\right] \geq \mathcal{F}\left[\mathbf{h}_{2,\text{RR2}}(\omega)\right] \geq \cdots \geq \mathcal{F}\left[\mathbf{h}_{M,\text{RR2}}(\omega)\right], \tag{51}$$

$$\mathcal{D}\left[\mathbf{h}_{1,\text{RR2}}(\omega)\right] \leq \mathcal{D}\left[\mathbf{h}_{2,\text{RR2}}(\omega)\right] \leq \cdots \leq \mathcal{D}\left[\mathbf{h}_{M,\text{RR2}}(\omega)\right]. \tag{52}$$

Now, let us consider a regularized version of $\mathbf{h}_{Q,\text{RR2}}(\omega)$, i.e.,

$$\mathbf{h}_{Q,\text{RR2},\epsilon}(\omega) = \frac{\mathbf{P}_{3,1:Q}(\omega)\mathbf{d}(\omega,0)}{\mathbf{d}^H(\omega,0)\mathbf{P}_{3,1:Q}(\omega)\mathbf{d}(\omega,0)}, \tag{53}$$

where

$$\mathbf{P}_{3,1:Q}(\omega) = \mathbf{T}_{1:Q}(\omega)\left[\mathbf{\Lambda}_{1:Q}(\omega)+\epsilon\mathbf{I}_Q\right]^{-1}\mathbf{T}_{1:Q}^H(\omega), \tag{54}$$

and $\epsilon \geq 0$ is the regularization parameter. It can be shown (see the Appendix) that $\mathcal{F}[\mathbf{h}_{Q,\text{RR2},\epsilon}(\omega)]$ is a decreasing function of Q, and an increasing function of ϵ [the upper bound is $\lambda_1(\omega)$]. Then, $\mathcal{D}[\mathbf{h}_{Q,\text{RR2},\epsilon}(\omega)]$ is an increasing function of Q, and a decreasing function of ϵ. We observe that the particular case of $Q=M$ and $\epsilon=\infty$ corresponds to the beamformer obtained from the maximization of $\mathcal{D}'[\mathbf{h}(\omega)]$ in Eq. (23), i.e.,

$$\mathbf{h}_{M,\text{RR2},\infty}(\omega) = \frac{\mathbf{\Gamma}_{\pi/2,\pi}^{-1}(\omega)\mathbf{d}(\omega,0)}{\mathbf{d}^H(\omega,0)\mathbf{\Gamma}_{\pi/2,\pi}^{-1}(\omega)\mathbf{d}(\omega,0)}. \tag{55}$$

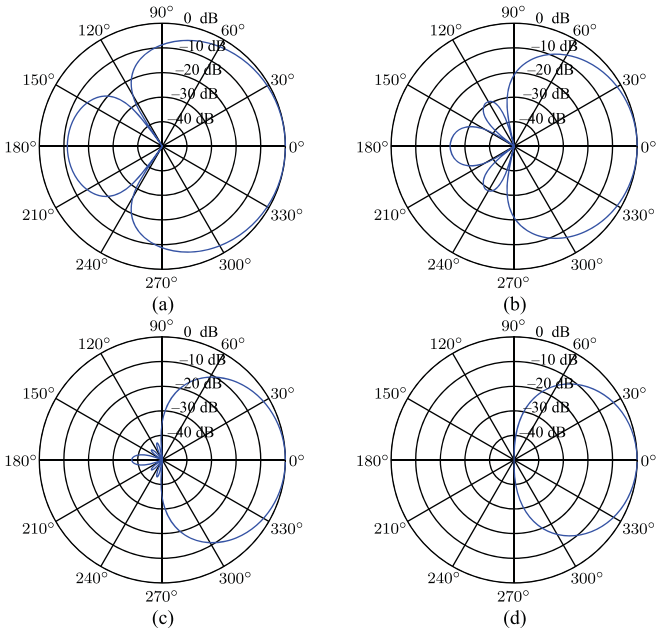

FIG. 1. (Color online) Beampatterns of the supercardioid beamformer, $\mathbf{h}_{\mathrm{SC}}(\omega)$, for different orders: (a) first-order, (b) second-order, (c) third-order, and (d) fourth-order. Conditions: $\delta = 1.0\,\mathrm{cm}$ and $f = 1\,\mathrm{kHz}$.

VI. GENERALIZATION

Here, we expand the definition of the FBR and separate the front from the back by some angle ψ. A more general definition of the FBR, named generalized FBR in this paper, is then

$$\mathcal{F}_{\psi}[\mathbf{h}(\omega)] = \frac{\mathbf{h}^H(\omega)\mathbf{\Gamma}_{0,\psi}(\omega)\mathbf{h}(\omega)}{\mathbf{h}^H(\omega)\mathbf{\Gamma}_{\psi,\pi}(\omega)\mathbf{h}(\omega)}, \tag{56}$$

where

$$\mathbf{\Gamma}_{0,\psi}(\omega) = \mathcal{N}_{0,\psi}\int_0^{\psi}\mathbf{d}(\omega,\theta)\mathbf{d}^H(\omega,\theta)\sin\theta d\theta, \tag{57}$$

$$\mathbf{\Gamma}_{\psi,\pi}(\omega) = \mathcal{N}_{\psi,\pi}\int_{\psi}^{\pi}\mathbf{d}(\omega,\theta)\mathbf{d}^H(\omega,\theta)\sin\theta d\theta. \tag{58}$$

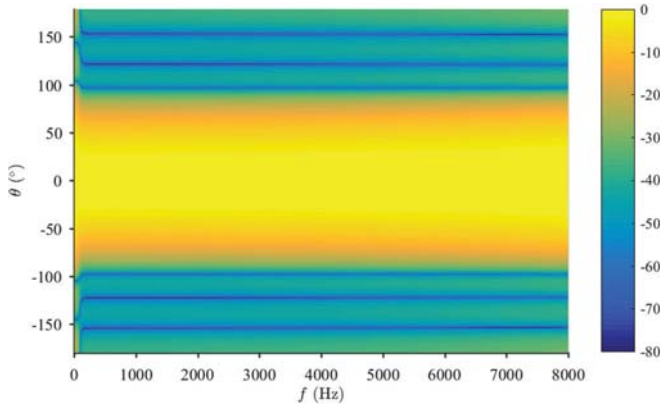

FIG. 2. Beampatterns of the third-order supercardioid beamformer, $\mathbf{h}_{\mathrm{SC}}(\omega)$, versus frequency. Conditions: $M = 4$ and $\delta = 1.0\,\mathrm{cm}$.

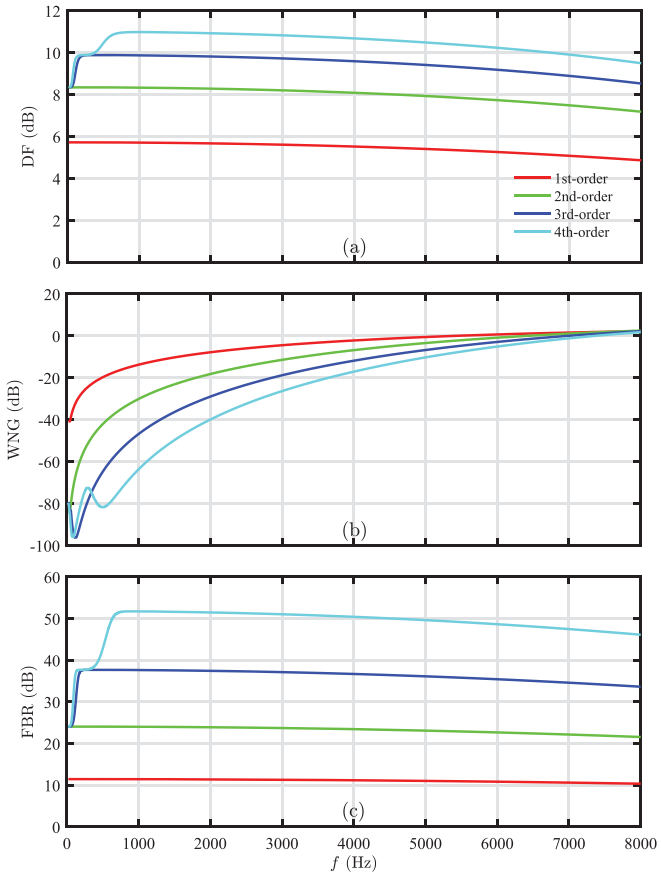

FIG. 3. Performance of the supercardioid beamformer, $\mathbf{h}_{\mathrm{SC}}(\omega)$, versus frequency for different orders: (a) DF, (b) WNG, and (c) FBR. Conditions: $\delta = 1.0\,\mathrm{cm}$.

A definition similar to Eq. (56) was presented in Sena *et al.* (2012) and Sena *et al.* (2011), but the optimization and implementation are done in a very much different way. Using Eq. (56), we can write the DF as

$$\mathcal{D}[\mathbf{h}(\omega)] = \frac{2\mathcal{N}_{0,\psi}\mathcal{N}_{\psi,\pi}\mathcal{D}'_{\psi}[\mathbf{h}(\omega)]}{\mathcal{N}_{0,\psi} + \mathcal{N}_{\psi,\pi}\mathcal{F}_{\psi}[\mathbf{h}(\omega)]}, \tag{59}$$

where

$$\mathcal{D}'_{\psi}[\mathbf{h}(\omega)] = \frac{|\mathbf{h}^H(\omega)\mathbf{d}(\omega,0)|^2}{\mathbf{h}^H(\omega)\mathbf{\Gamma}_{\psi,\pi}(\omega)\mathbf{h}(\omega)}. \tag{60}$$

We can jointly diagonalize the two Hermitian matrices $\mathbf{\Gamma}_{0,\psi}(\omega)$ and $\mathbf{\Gamma}_{\psi,\pi}(\omega)$ as

$$\mathbf{T}_{\psi}^H(\omega)\mathbf{\Gamma}_{0,\psi}(\omega)\mathbf{T}_{\psi}(\omega) = \mathbf{\Lambda}_{\psi}(\omega), \tag{61}$$

$$\mathbf{T}_{\psi}^H(\omega)\mathbf{\Gamma}_{\psi,\pi}(\omega)\mathbf{T}_{\psi}(\omega) = \mathbf{I}_M, \tag{62}$$

where

$$\mathbf{T}_{\psi}(\omega) = \left[\mathbf{t}_{\psi,1}(\omega)\,\mathbf{t}_{\psi,2}(\omega)\,\cdots\,\mathbf{t}_{\psi,M}(\omega)\right] \tag{63}$$

and

$$\Lambda_{\psi}(\omega) = \mathrm{diag}\left[\lambda_{\psi,1}(\omega), \lambda_{\psi,2}(\omega), \ldots, \lambda_{\psi,M}(\omega)\right] \tag{64}$$

are the eigenvector and eigenvalue matrices of $\mathbf{\Gamma}_{\psi,\pi}^{-1}(\omega)\mathbf{\Gamma}_{0,\psi}(\omega)$, respectively, and organized similarly to $\mathbf{\Lambda}(\omega)$ and $\mathbf{T}(\omega)$. So, we have

$$\mathbf{T}_{\psi}^{H}(\omega)\mathbf{\Gamma}_{0,\pi}(\omega)\mathbf{T}_{\psi}(\omega)=\frac{1}{2\mathcal{N}_{0,\psi}}\Lambda_{\psi}(\omega)+\frac{1}{2\mathcal{N}_{\psi,\pi}}\mathbf{I}_{M}. \tag{65}$$

Following the same steps as in Sec. V C, we can find a more general reduced-rank filter,

$$\mathbf{h}_{Q,\psi}(\omega)=\frac{\mathbf{P}_{4,1:Q}(\omega)\mathbf{d}(\omega,0)}{\mathbf{d}^{H}(\omega,0)\mathbf{P}_{4,1:Q}(\omega)\mathbf{d}(\omega,0)}, \tag{66}$$

where

$$\mathbf{P}_{4,1:Q}(\omega)=\mathbf{T}_{\psi,1:Q}(\omega)\times\left[\mathbf{T}_{\psi,1:Q}^{H}(\omega)\mathbf{T}_{\psi,1:Q}(\omega)\right]^{-1}\mathbf{T}_{\psi,1:Q}^{H}(\omega), \tag{67}$$

and $\mathbf{T}_{\psi,1:Q}(\omega)$ is defined in a similar way to $\mathbf{T}_{1:Q}(\omega)$. For $Q=1$, we get

$$\mathbf{h}_{1,\psi}(\omega)=\frac{\mathbf{t}_{\psi,1}(\omega)}{\mathbf{d}^{H}(\omega,0)\mathbf{t}_{\psi,1}(\omega)}, \tag{68}$$

which is the beamformer obtained from maximization of $\mathcal{F}_{\psi}[\mathbf{h}(\omega)]$.

From the maximization of the DF in (59), we can derive another reduced-rank filter,

$$\mathbf{h}_{Q,2,\psi}(\omega)=\frac{\mathbf{P}_{5,1:Q}(\omega)\mathbf{d}(\omega,0)}{\mathbf{d}^{H}(\omega,0)\mathbf{P}_{5,1:Q}(\omega)\mathbf{d}(\omega,0)}, \tag{69}$$

where

$$\mathbf{P}_{5,1:Q}(\omega)=\mathbf{T}_{\psi,1:Q}(\omega)\times\left[\frac{1}{\mathcal{N}_{0,\psi}}\mathbf{\Lambda}_{\psi,1:Q}(\omega)+\frac{1}{\mathcal{N}_{\psi,\pi}}\mathbf{I}_{Q}\right]^{-1}\mathbf{T}_{\psi,1:Q}^{H}(\omega), \tag{70}$$

and $\mathbf{\Lambda}_{\psi,1:Q}(\omega)$ is defined analogously to $\mathbf{\Lambda}_{1:Q}(\omega)$. It can be verified that (see the Appendix)

$$\mathcal{F}\left[\mathbf{h}_{1,2,\psi}(\omega)\right]\geq\mathcal{F}\left[\mathbf{h}_{2,2,\psi}(\omega)\right]\geq\cdots\geq\mathcal{F}\left[\mathbf{h}_{M,2,\psi}(\omega)\right], \tag{71}$$

$$\mathcal{D}\left[\mathbf{h}_{1,2,\psi}(\omega)\right]\leq\mathcal{D}\left[\mathbf{h}_{2,2,\psi}(\omega)\right]\leq\cdots\leq\mathcal{D}\left[\mathbf{h}_{M,2,\psi}(\omega)\right]. \tag{72}$$

We can also construct a regularized version of $\mathbf{h}_{Q,2,\psi}(\omega)$, i.e.,

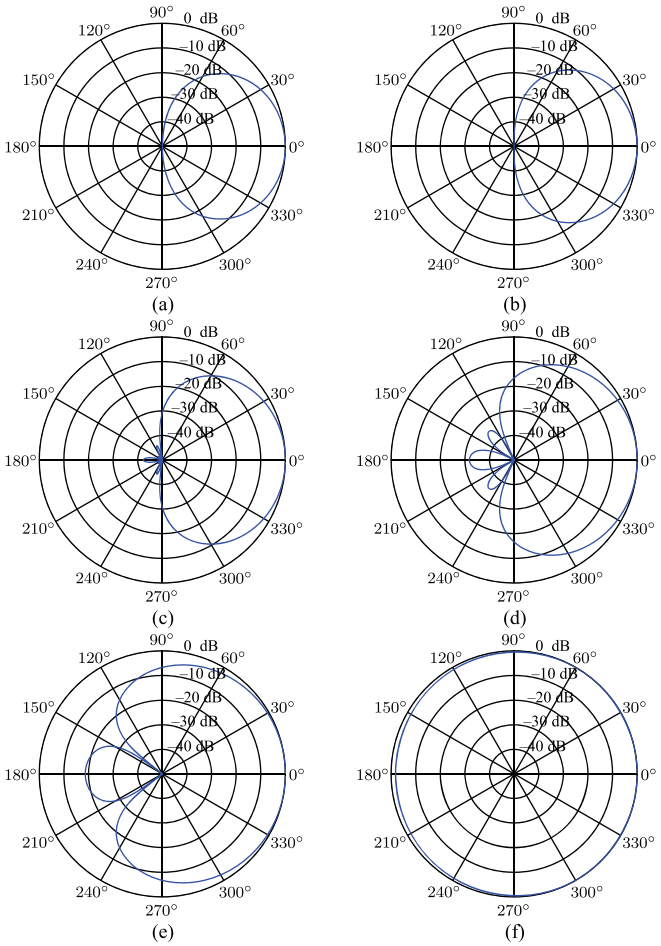

FIG. 4. (Color online) Beampatterns of the beamformer $\mathbf{h}_{Q,\mathrm{RR}}(\omega)$ for different values of Q: (a) $Q=1$, (b) $Q=2$, (c) $Q=3$, (d) $Q=4$, (e) $Q=5$, and (f) $Q=6$. Conditions: $M=6$, $\delta=1.0$ cm, and $f=1$ kHz.

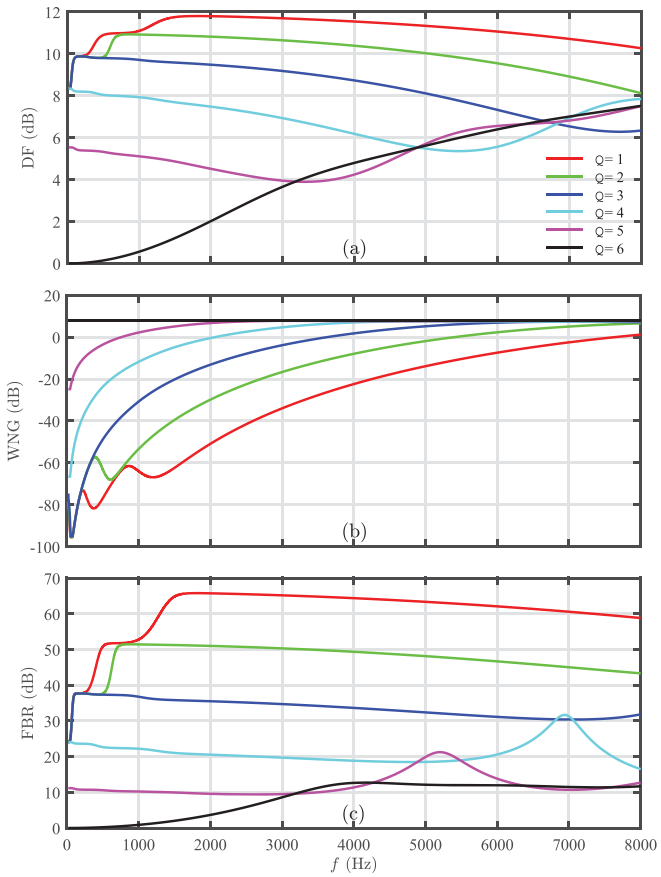

FIG. 5. Performance of the beamformer $\mathbf{h}_{Q,\mathrm{RR}}(\omega)$ versus frequency for different values of Q: (a) DF, (b) WNG, and (c) FBR. Conditions: $M=6$ and $\delta=1.0$ cm.

$$\mathbf{h}_{Q,2,\psi,\epsilon}(\omega)=\frac{\mathbf{P}_{6,1:Q}(\omega)\mathbf{d}(\omega,0)}{\mathbf{d}^H(\omega,0)\mathbf{P}_{6,1:Q}(\omega)\mathbf{d}(\omega,0)}, \tag{73}$$

where

$$\mathbf{P}_{6,1:Q}(\omega)=\mathbf{T}_{\psi,1:Q}(\omega)\times\left[\frac{1}{\mathcal{N}_{0,\psi}}\mathbf{\Lambda}_{\psi,1:Q}(\omega)+\frac{\epsilon}{\mathcal{N}_{\psi,\pi}}\mathbf{I}_Q\right]^{-1}\mathbf{T}^H_{\psi,1:Q}(\omega). \tag{74}$$

The relations between $\mathcal{D}[\mathbf{h}_{Q,2,\psi,\epsilon}(\omega)]$, $\mathcal{F}_\psi[\mathbf{h}_{Q,2,\psi,\epsilon}(\omega)]$, and Q and ϵ are similar to those with the beamformer $\mathbf{h}_{Q,\mathrm{RR2},\epsilon}(\omega)$. The particular case of $Q=M$ and $\epsilon=\infty$ corresponds to the beamformer obtained from maximization of $\mathcal{D}'_\psi[\mathbf{h}(\omega)]$ in Eq. (60), i.e.,

$$\mathbf{h}_{M,2,\psi,\infty}(\omega)=\frac{\mathbf{\Gamma}^{-1}_{\psi,\pi}(\omega)\mathbf{d}(\omega,0)}{\mathbf{d}^H(\omega,0)\mathbf{\Gamma}^{-1}_{\psi,\pi}(\omega)\mathbf{d}(\omega,0)}. \tag{75}$$

VII. SIMULATIONS

In this section, the performance of the proposed beamformers are evaluated in terms of beampattern, WNG, DF, and FBR/GFBR.

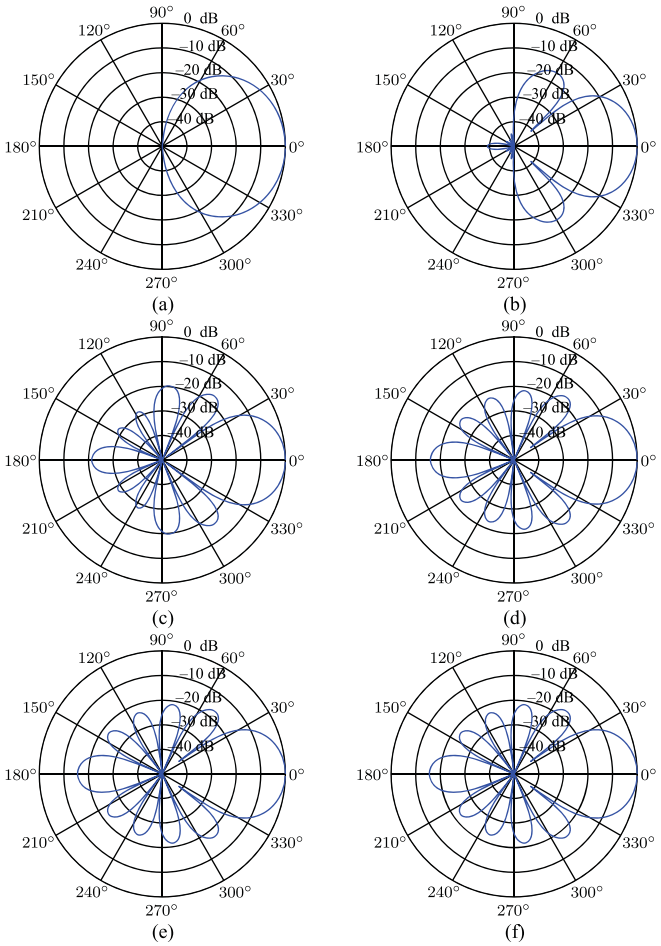

FIG. 6. (Color online) Beampatterns of the beamformer $\mathbf{h}_{Q,\mathrm{RR2}}(\omega)$ for different values of Q: (a) $Q=1$, (b) $Q=2$, (c) $Q=3$, (d) $Q=4$, (e) $Q=5$, and (f) $Q=6$. Conditions: $M=6$, $\delta=1.0\,\mathrm{cm}$, and $f=1\,\mathrm{kHz}$.

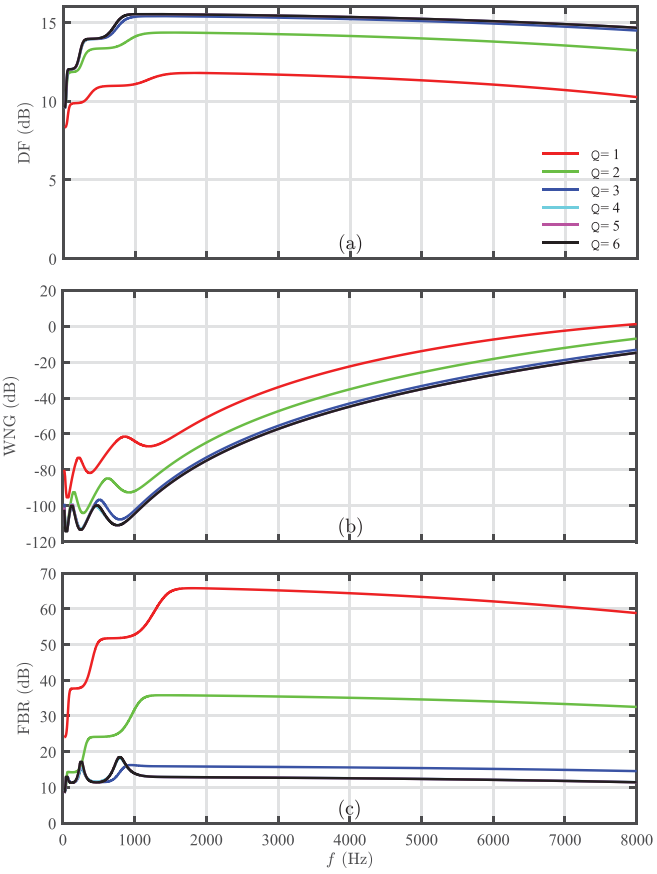

FIG. 7. Performance of the beamformer $\mathbf{h}_{Q,\mathrm{RR2}}(\omega)$ versus frequency for different values of Q: (a) DF, (b) WNG, and (c) FBR. Conditions: $M=6$ and $\delta=1.0\,\mathrm{cm}$.

A. Performance of the supercardioid beamformer

First, we investigate the performance of the supercardioid beamformer. Figure 1 plots the beampatterns of this

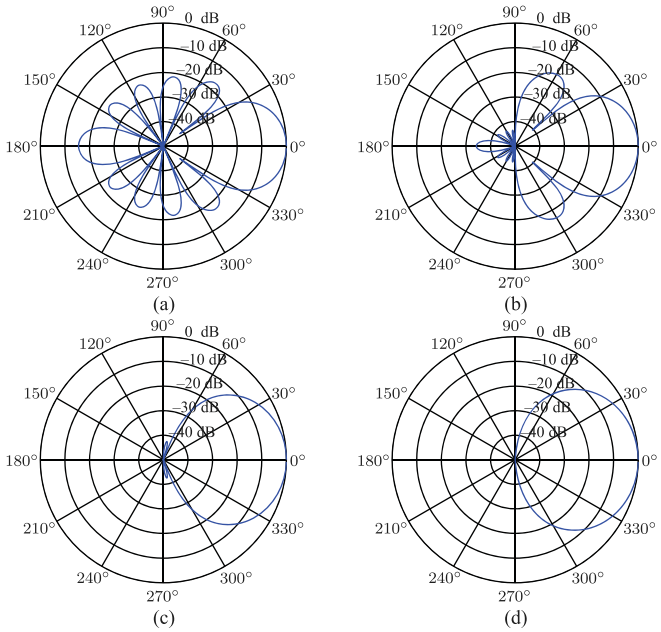

FIG. 8. (Color online) Beampatterns of the beamformer $\mathbf{h}_{Q,\mathrm{RR2},\epsilon}(\omega)$ for different values of ϵ: (a) $\epsilon=10^0$, (b) $\epsilon=10^2$, (c) $\epsilon=10^4$, and (d) $\epsilon=10^6$. Conditions: $M=6$, $Q=6$, $\delta=1.0\,\mathrm{cm}$, and $f=1\,\mathrm{kHz}$.

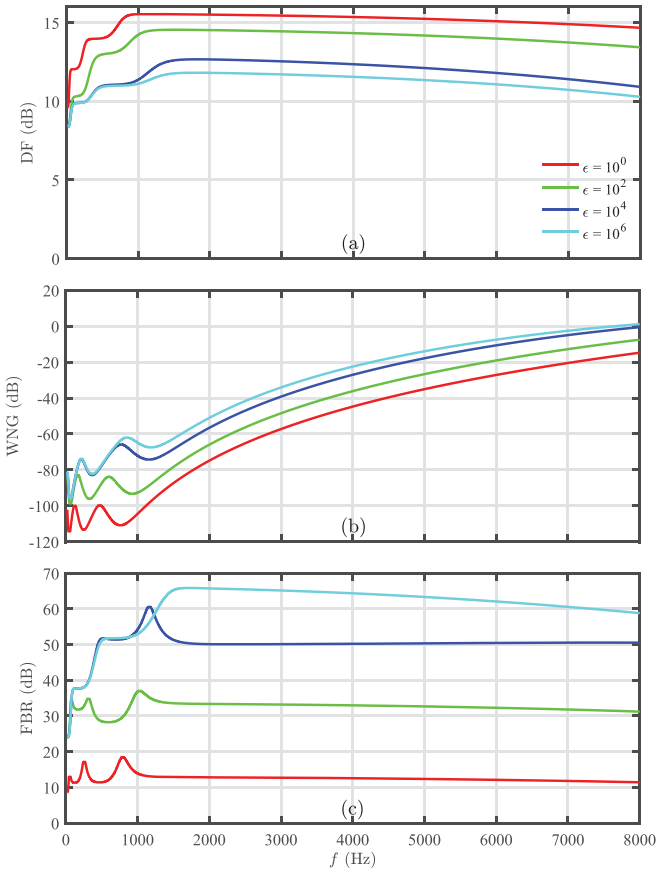

FIG. 9. Performance of the beamformer $\mathbf{h}_{Q,\mathrm{RR2},\epsilon}(\omega)$ versus frequency for different values of ϵ: (a) DF, (b) WNG, and (c) FBR. Conditions: $M=6$, $Q=6$, and $\delta=1.0$ cm.

beamformer for different orders at $f=1$ kHz. Figure 2 plots the beampatterns of the third-order supercardioid beamformer versus frequency. As can be seen, the obtained beampatterns are almost frequency invariant, except at very low

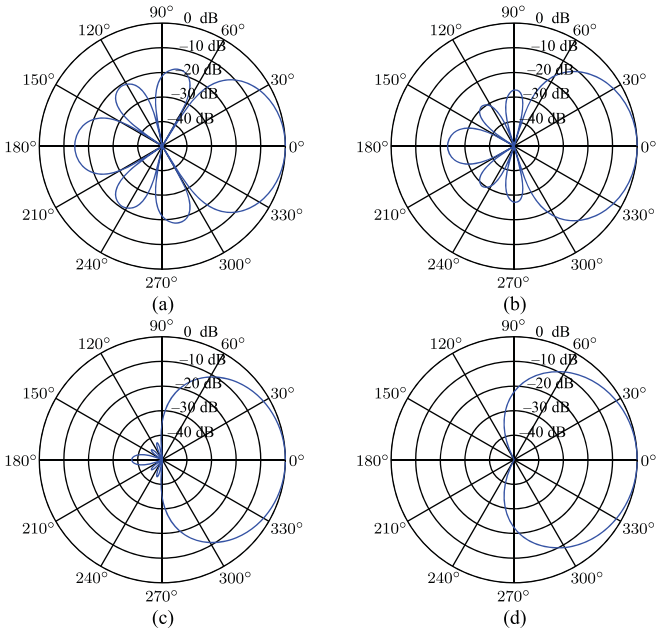

FIG. 10. (Color online) Beampatterns of the beamformer $\mathbf{h}_{Q,\psi}(\omega)$ with different values of ψ: (a) $\psi=30°$, (b) $\psi=60°$, (c) $\psi=90°$, and (d) $\psi=120°$. Conditions: $M=4$, $Q=1$, $\delta=1.0$ cm, and $f=1$ kHz.

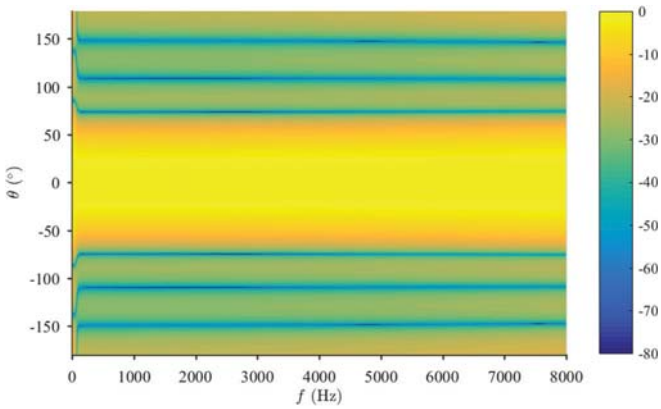

FIG. 11. Beampatterns of the beamformer $\mathbf{h}_{Q,\psi}(\omega)$ versus frequency. Conditions: $M=4$, $\psi=60°$, $Q=1$, and $\delta=1.0$ cm.

frequencies ($f<150$ Hz) due to numerical problems. The DF, WNG, and FBR of the supercardioid beamformer versus frequency for different orders are plotted in Fig. 3. One can see from this figure that the DF and FBR increase with the order, while the WNG decreases. Even though the supercardioid beamformer can achieve maximum FBR, it suffers from white noise amplification (very low WNG), and its DF is also limited, which motivated us to develop the $\mathbf{h}_{Q,\mathrm{RR}}(\omega)$ and $\mathbf{h}_{Q,\mathrm{RR2}}(\omega)$ beamformers.

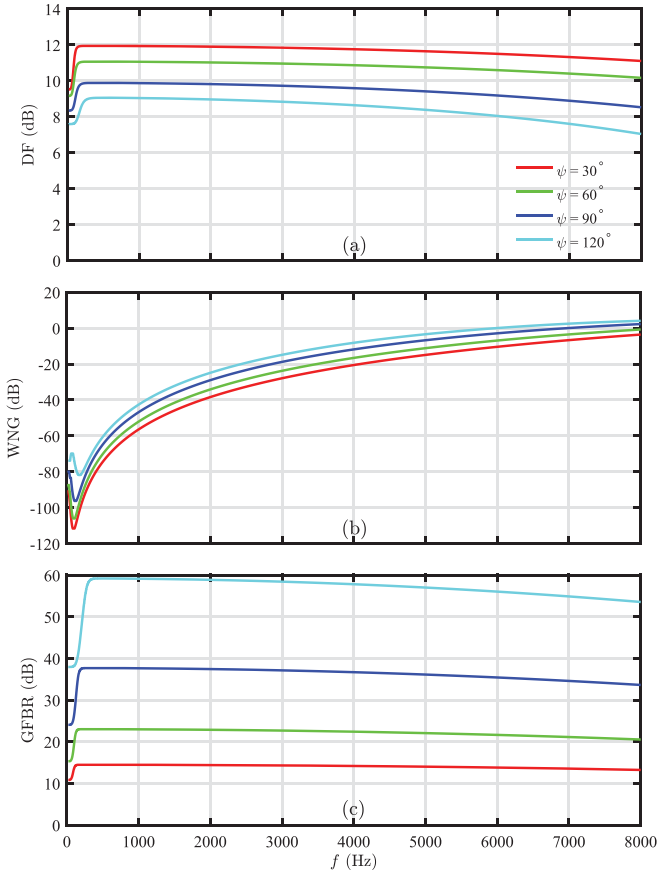

FIG. 12. Performance of the beamformer $\mathbf{h}_{Q,\psi}(\omega)$ with different values of ψ: (a) DF, (b) WNG, and (c) GFBR. Conditions: $M=4$, $Q=1$, and $\delta=1.0$ cm.

B. Performance of the reduced-rank beamformers

In this subsection, the performance of the beamformer $\mathbf{h}_{Q,\mathrm{RR}}(\omega)$ is investigated. We consider a ULA with $M=6$ and $\delta=1.0\,\mathrm{cm}$. Figure 4 plots the beampatterns of $\mathbf{h}_{Q,\mathrm{RR}}(\omega)$ for $f=1\,\mathrm{kHz}$ and different values of Q. As we can see, the beampatterns of this beamformer vary significantly with Q. The beamwidth increases with the value of Q. When $Q=1$, we obtain the beampattern of the fifth-order supercardioid beamformer, while when $Q=6$, we get the beampattern of the DS beamformer. The DF, WNG, and FBR of $\mathbf{h}_{Q,\mathrm{RR}}(\omega)$ as a function of frequency for different values of Q are plotted in Fig. 5. The beamformer $\mathbf{h}_{Q,\mathrm{RR}}(\omega)$ achieves the maximum FBR and high DF when $Q=1$, but it suffers from white noise amplification in this case, which is particularly serious at low frequencies. When $Q=6$, however, it obtains the maximum WNG, but the FBR and DF are limited. From Fig. 5, one can see that the WNG of the beamformer $\mathbf{h}_{Q,\mathrm{RR}}(\omega)$ increases while the DF and FBR decrease with the value of Q, which should be expected due to the form of $\mathbf{h}_{Q,\mathrm{RR}}(\omega)$ in Eq. (34), except for some disturbances of the DF and FBR at high frequencies. Clearly, the beamformer $\mathbf{h}_{Q,\mathrm{RR}}(\omega)$ can achieve some tradeoff between the DF, FBR, and WNG by adjusting the value of Q.

Next, we examine the performance of the beamformer $\mathbf{h}_{Q,\mathrm{RR2}}(\omega)$. Again, a ULA with $M=6$ and $\delta=1.0\,\mathrm{cm}$ is considered. The beampatterns of $\mathbf{h}_{Q,\mathrm{RR2}}(\omega)$ are plotted in Fig. 6 for $f=1\,\mathrm{kHz}$ and different values of Q. As can be seen, the beampatterns of this beamformer vary greatly with Q also. The beamwidth decreases with the increase of Q. When $Q=1$ and 6, we get the beampatterns of the fifth-order supercardioid beamformer and classical superdirective beamformer (fifth-order hypercardioid), respectively. Figure 7 plots the DF, WNG, and FBR of $\mathbf{h}_{Q,\mathrm{RR2}}(\omega)$ versus frequency for different values of Q. The WNG and FBR of $\mathbf{h}_{Q,\mathrm{RR2}}(\omega)$ decrease with the increase of the value of Q, while the DF increases, which is consistent with the analysis, except for some disturbances of the FBR at low frequencies due to some numerical problems. Some of the curves are very close to each other, since the performances of the beamformer $\mathbf{h}_{Q,\mathrm{RR2}}(\omega)$ when $Q\geq 4$ are similar for the given microphone array, which can also be observed from the beampatterns in Fig. 6. The beampatterns of $\mathbf{h}_{Q,\mathrm{RR2},\epsilon}(\omega)$ are plotted in Fig. 8 for $Q=6$, $f=1\,\mathrm{kHz}$, and different values of ϵ. Obviously, when $\epsilon=1$, we have the beampattern of the classical superdirective beamformer, and when $\epsilon=10^6$, the obtained beampattern is very close to that of the fifth-order supercardioid beamformer. Figure 9 plots the DF, WNG, and FBR of $\mathbf{h}_{Q,\mathrm{RR2},\epsilon}(\omega)$ versus frequency for $Q=6$ and different

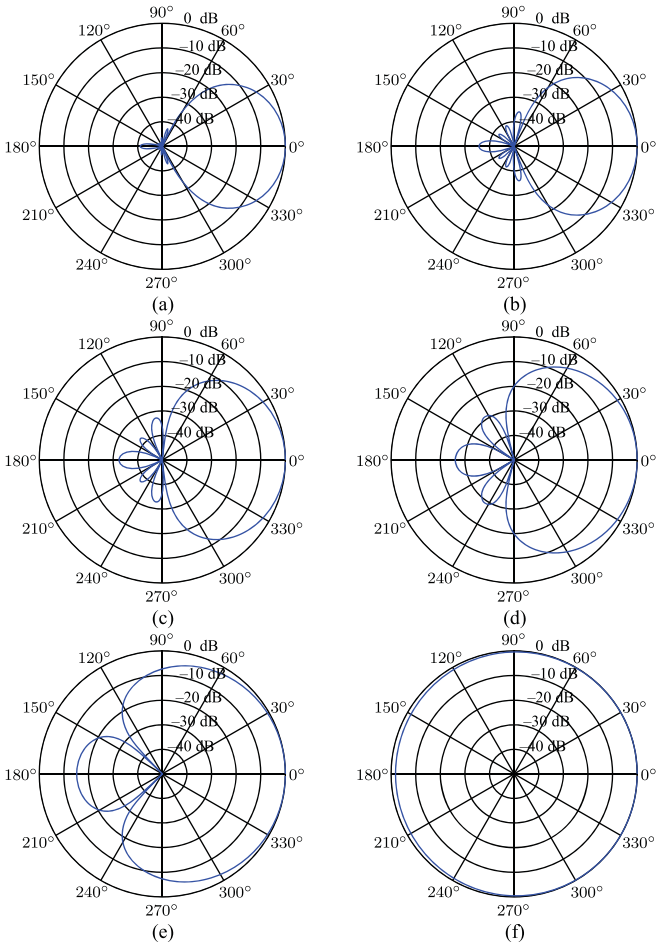

FIG. 13. (Color online) Beampatterns of the beamformer $\mathbf{h}_{Q,\psi}(\omega)$ for different values of Q: (a) $Q=1$, (b) $Q=2$, (c) $Q=3$, (d) $Q=4$, (e) $Q=5$, and (f) $Q=6$. Conditions: $M=6$, $\psi=60^\circ$, $\delta=1.0\,\mathrm{cm}$, and $f=1\,\mathrm{kHz}$.

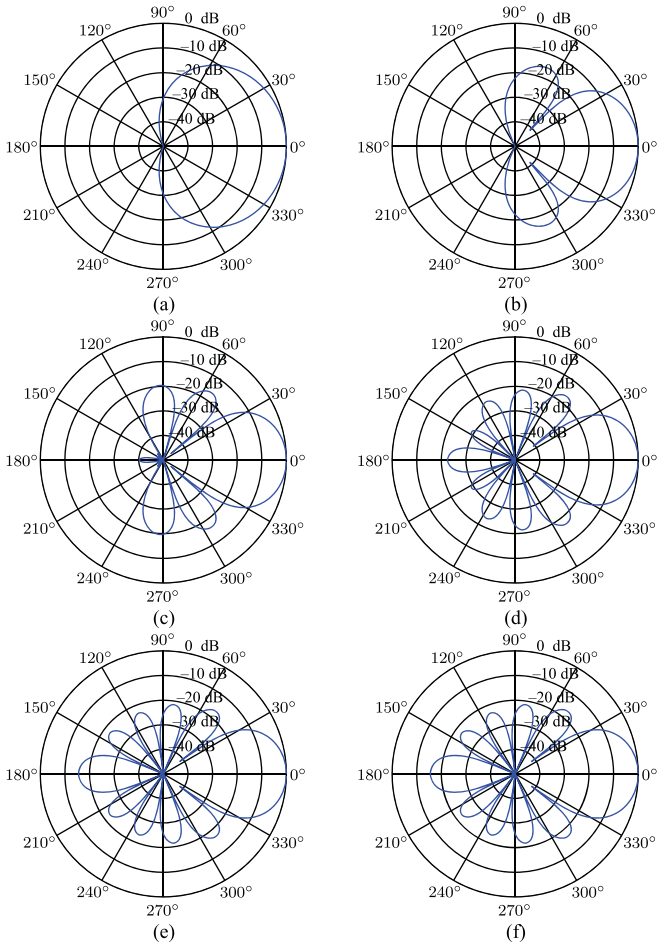

FIG. 14. (Color online) Beampatterns of the beamformer $\mathbf{h}_{Q,2,\psi}(\omega)$ for different values of Q: (a) $Q=1$, (b) $Q=2$, (c) $Q=3$, (d) $Q=4$, (e) $Q=5$, and (f) $Q=6$. Conditions: $M=6$, $\psi=120^\circ$, $\delta=1.0\,\mathrm{cm}$, and $f=1\,\mathrm{kHz}$.

values of ϵ. As can be seen, the WNG and FBR increase with ϵ, while the DF decreases, which is consistent with the analysis, except for the FBR at low frequency bands.

C. Performance of the beamformers derived from GFBR

Now, we consider a ULA with $M=4$ and $\delta=1.0\,\text{cm}$. The beampatterns of $\mathbf{h}_{Q,\psi}(\omega)$ for $Q=1$, $f=1\,\text{kHz}$, and different values of ψ are plotted in Fig. 10. As seen, the beamwidth of the beampattern increases with the value of ψ. Accordingly, the beamwidth of the designed beampattern can be controlled by adjusting the value of ψ indirectly. It should be noted that for the given microphone array with $M=4$ and $\delta=1\,\text{cm}$, the beamwidth of the designed beampattern cannot be very narrow, even when $\psi \to 0^\circ$, due to the small aperture of the array. As the value of ψ increases, the beamwidth of $\mathbf{h}_{1,\psi}(\omega)$ gradually approaches to 2ψ. The beampatterns of $\mathbf{h}_{1,\psi}(\omega)$ versus frequency for $\psi=60^\circ$ are presented in Fig. 11. It can be seen that the obtained beampatterns are almost frequency invariant. The DF, WNG, and GFBR of $\mathbf{h}_{1,\psi}(\omega)$ versus frequency for different values of ψ are plotted in Fig. 12. We observe that the DF decreases with the increase of the value of ψ. This is reasonable since the larger is the beamwidth, the smaller is the DF. The values of WNG and GFBR increase with the value of ψ.

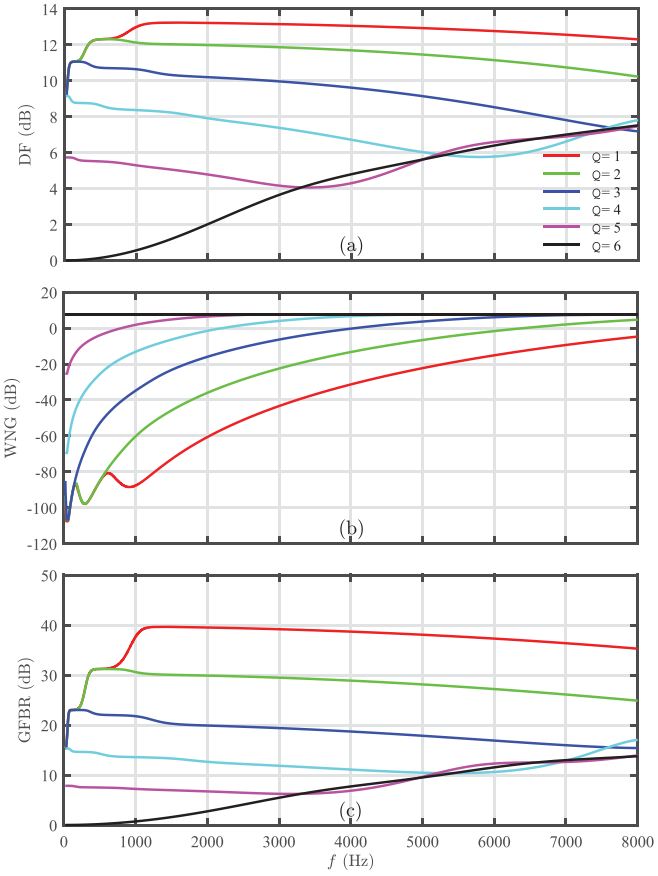

FIG. 15. Performance of the beamformer $\mathbf{h}_{Q,\psi}(\omega)$ versus frequency for different values of Q: (a) DF, (b) WNG, and (c) GFBR. Conditions: $M=6$, $\psi=60^\circ$, and $\delta=1.0\,\text{cm}$.

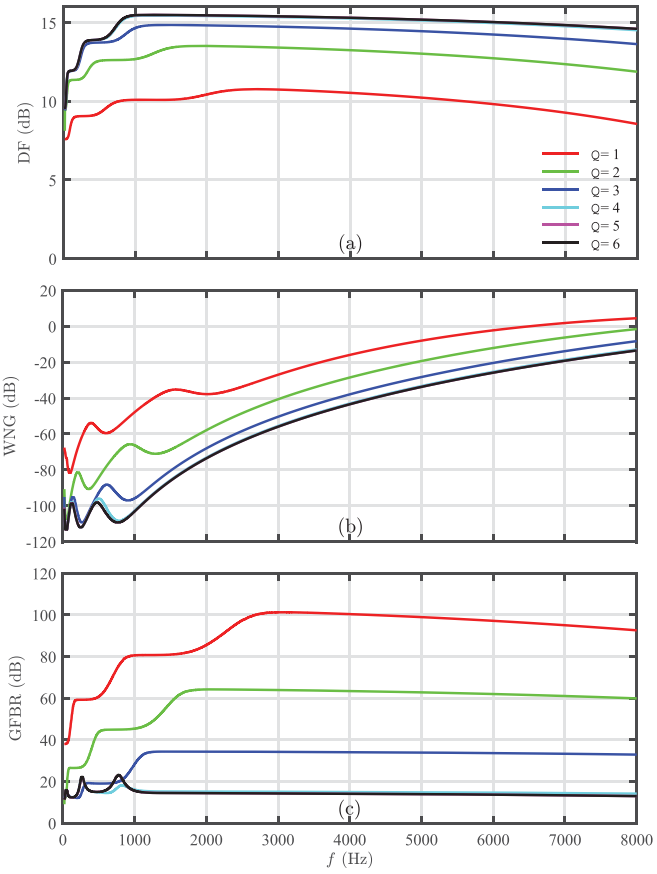

FIG. 16. Performance of the beamformer $\mathbf{h}_{Q,2,\psi}(\omega)$ versus frequency for different values of Q: (a) DF, (b) WNG, and (c) GFBR. Conditions: $M=6$, $\psi=120^\circ$, and $\delta=1.0\,\text{cm}$.

Then, a ULA with $M=6$ and $\delta=1.0\,\text{cm}$ is considered. Figures 13 and 14 plot the beampatterns of $\mathbf{h}_{Q,\psi}(\omega)$ ($\psi=60^\circ$) and $\mathbf{h}_{Q,2,\psi}(\omega)$ ($\psi=120^\circ$), respectively, for $f=1\,\text{kHz}$ and different values of Q. The beamwidth of $\mathbf{h}_{Q,\psi}(\omega)$ increases while the beamwidth of $\mathbf{h}_{Q,2,\psi}(\omega)$ decreases as the value of Q increases. The DF, WNG, and GFBR of $\mathbf{h}_{Q,\psi}(\omega)$

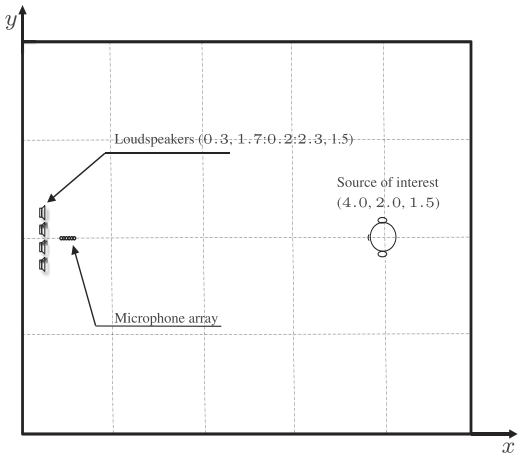

FIG. 17. Floor layout of the simulation: the size of the room is 5 m × 4 m ×3 m (length × width × height), the microphone array consists of six microphones, which are placed, respectively, at (0.50: 0.02: 0.60, 2.0, 1.5), a loudspeaker is placed at (4.0, 2.0, 1.5) is to simulate the source of interest, and four loudspeakers are placed at (0.3, 1.7: 0.2: 2.3, 1.5) to simulate interference sources.

and $\mathbf{h}_{Q,2,\psi}(\omega)$ as a function of frequency for different values of Q are plotted in Figs. 15 and 16, respectively. The trends of the DF, WNG, and GFBR versus the parameter Q agree well with the analysis, except for some disturbances at low frequencies due to numerical problems. It is clearly seen that these developed beamformers facilitate tradeoffs among the DF, WNG, and GFBR by adjusting the value of Q.

D. Performance in simulated reverberant room environments

Finally, the performance of the developed beamformers are evaluated in room acoustic environments simulated with the widely used image model (Allen and Berkley, 1979; Lehmanna and Johansson, 2008). The size of the simulated room is 5 m × 4 m × 3 m (length × width × height). For convenience of exposition, we denote the position in the room as (x, y, z) with reference to a corner in a Cartesian coordinate system. A microphone array consisting of six omnidirectional microphones is used and the positions of the six microphones are at (0.50: 0.02: 0.60, 2.0, 1.5) as illustrated in Fig. 17. A loudspeaker, playing back a pre-recorded speech signal, is placed at (4.0, 2.0, 1.5) to simulate a source of interest. Four loudspeakers (e.g., from the sound bar of a television) placed at (0.3, 1.7: 0.2: 2.3, 1.5) are used to simulate interference sources. The room impulse responses (RIRs) from every loudspeaker to the six microphones are generated with the image model method (Allen and Berkley, 1979; Lehmanna and Johansson, 2008). The reflection coefficients of all the six walls at set to 0.35 and the corresponding reverberation time T_{60}, i.e., the time for the sound to die away to a level 60 decibels below its original level, which is measured by the Schroeder's method (Schroeder, 1965), is approximately 100 ms. The output signals of the microphones are generated by convolving the source signal (pre-recorded with a sampling rate of 16 kHz from a female speaker in a quiet environment) with the RIRs from the position of the source of interest to the array of microphones, and then adding either spatially and temporally white Gaussian noise or interference signals (generated by convolving another pre-recorded clean speech signal or white Gaussian noise with the RIRs from the positions of the four interference loudspeakers to the array of microphones).

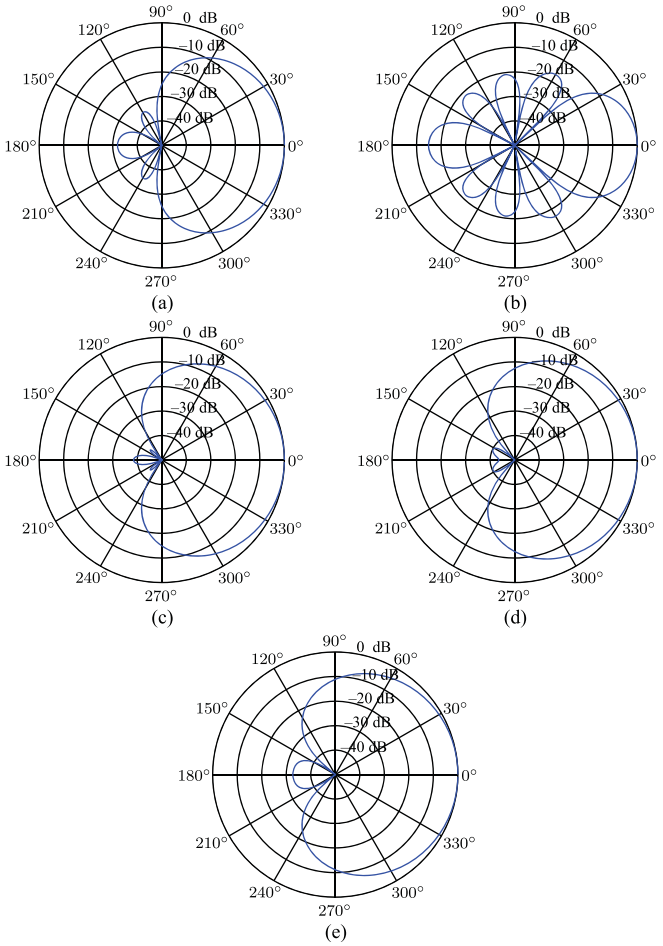

FIG. 18. (Color online) Beampatterns at 1 kHz of (a) the fifth-order $\mathbf{h}_{SC}(\omega)$, (b) the fifth-order $\mathbf{h}_{S}(\omega)$, (c) $\mathbf{h}_{Q,\psi}(\omega)$ with $Q=1$ and $\psi=120°$, (d) $\mathbf{h}_{Q,\psi}(\omega)$ with $Q=2$ and $\psi=120°$, and (e) $\mathbf{h}_{Q,\psi}(\omega)$ with with $Q=3$ and $\psi=120°$.

TABLE I. The DF values of the five compared beamformers (computed at 1 kHz).

			$\mathbf{h}_{Q,\psi}(\omega)$ with $\psi=120°$		
Beamformers	$\mathbf{h}_{SC}(\omega)$	$\mathbf{h}_{S}(\omega)$	$Q=1$	$Q=2$	$Q=3$
DF	8.34 dB	9.78 dB	7.43 dB	7.23 dB	5.02 dB

Based on the previous simulations, we investigate and compare the following beamformers: the fifth-order supercardiord beamformer $\mathbf{h}_{SC}(\omega)$, the fifth-order superdirective beamformer $\mathbf{h}_{S}(\omega)$, and the reduced-rank beamformer $\mathbf{h}_{Q,\psi}(\omega)$ with three cases, i.e., $Q=1$ and $\psi=120°$, $Q=2$ and $\psi=120°$, and $Q=3$ and $\psi=120°$. During implementation, the matrix $\mathbf{\Gamma}_{\psi,\pi}(\omega)$ is diagonally loaded with $10^{-5}\mathbf{I}_M$ for numerical stability where $\mathbf{I}_M$ is an identity matrix of size $M\times M$. The beampatterns at 1 kHz of these beamformers are plotted in Fig. 18. The values of the DF of these five beamformers, which are computed at 1 kHz, are listed in Table I.

Besides the beampattern and DF, we also investigate the array performance in the presence of white Gaussian noise, interference, and reverberation. We divide the RIRs into two parts: direct path and reflections, based on which we defined three metrics, i.e., the direct-path-signal-to-noise ratio (DSNR), the direct-path-signal-to-interference ratio (DSIR),

TABLE II. Performance of different beamformers. Conditions: $T_{60}\sim 100$ ms, $M=6$ and $\delta=2.0$ cm, the input DSNR, DSIR, and DSRR are, respectively, 10, 0, and 1.2 dB.

	Output performance (in dB)			
Beamformer	DSIR[a]	DSIR[b]	DSRR	DSNR
$\mathbf{h}_{SC}(\omega)$	20.12	18.49	5.86	1.25
$\mathbf{h}_{S}(\omega)$	16.19	13.02	**9.49**	−12.54
$\mathbf{h}_{Q,\psi}(\omega)$, $Q=1$, $\psi=120°$	**23.05**	**21.68**	5.10	1.91
$\mathbf{h}_{Q,\psi}(\omega)$, $Q=2$, $\psi=120°$	19.68	16.03	4.58	11.06
$\mathbf{h}_{Q,\psi}(\omega)$, $Q=3$, $\psi=120°$	18.44	14.40	4.48	**15.58**

[a]The case with the interference generated using a white Gaussian noise signal.
[b]The case with the interference generated using a speech signal.

direct-path-signal-to-reverberation ratio (DSRR). The input DSNR and DSIR in this simulation are set to 10 and 0 dB, respectively. The input DSRR for our simulation setup is approximately 1.2 dB. To compute the output DSNR, DSIR, and DSRR, we first divide the array output signals into frames with a frame size of 256 samples (16-ms long) and an overlap factor of 75%. The Kaiser window is applied to each frame to deal with the frequency aliasing problem. Then, a 256-point fast Fourier transform (FFT) is applied to the windowed signal frame to transform the array signal into the short-time Fourier transform (STFT) domain. In every STFT subband, a beamformer filter is designed and applied to the array signals. The inverse STFT (ISTFT) and overlap-add method are used to convert the processed signals back to the time domain. We finally compute the output DSNR, DSIR, and DSRR. We consider two cases. In the first one, the interference signals are generated by convolving a white Gaussian noise signal with the RIRs from the four interference loudspeakers to the microphones. In the second case, the interference signals are generated by convolving a speech signal (different from the source one) with the RIRs from the four interference loudspeakers to the microphones. The results of this case are summarized in Table II.

It is clearly seen from Table II the advantage of the reduced rank beamformers.

VIII. CONCLUSIONS

Exploiting the performance measures FBR and GFBR, we derived several kinds of beamformers, i.e., $\mathbf{h}_{\mathrm{SC}}(\omega)$, $\mathbf{h}_{Q,\mathrm{RR}}(\omega)$, $\mathbf{h}_{Q,\mathrm{RR2}}(\omega)$, $\mathbf{h}_{Q,\mathrm{RR2},\epsilon}(\omega)$, $\mathbf{h}_{Q,\psi}(\omega)$, $\mathbf{h}_{Q,2,\psi}(\omega)$, and $\mathbf{h}_{Q,2,\psi,\epsilon}(\omega)$. The beamformers $\mathbf{h}_{\mathrm{SC}}(\omega)$ and $\mathbf{h}_{1,\psi}(\omega)$ maximize the FBR and GFBR, respectively, and have almost frequency-invariant beampatterns. The beamwidth of the beamformer $\mathbf{h}_{1,\psi}(\omega)$ can be changed by adjusting the value of ψ. The other beamformers enable us to compromise between the FBR/GFBR and WNG or DF by adjusting the values of the parameters Q and/or ϵ. The DS and classical superdirective beamformers are particular cases of the proposed framework.

ACKNOWLEDGMENTS

This work was supported by the Israel Science Foundation (Grant No. 576/16), and the ISF-NSFC joint research program (Grant Nos. 2514/17 and 61761146001), and the NSFC Distinguished Young Scientists Fund (Grant No. 61425005). The work of X.W. was supported in part by the China Scholarship Council.

APPENDIX

$$\begin{aligned}\mathcal{D}(\mathbf{h}_{Q,2,\psi,\epsilon}) &= \frac{\left[\mathbf{d}^H(0)\mathbf{T}_{\psi,1:Q}\left(\frac{1}{\mathcal{N}_{0,\psi}}\mathbf{\Lambda}_{\psi,1:Q}+\frac{\epsilon}{\mathcal{N}_{\psi,\pi}}\mathbf{I}_Q\right)^{-1}\mathbf{T}_{\psi,1:Q}^H\mathbf{d}(0)\right]^2}{\mathbf{d}^H(0)\mathbf{T}_{\psi,1:Q}\left(\frac{1}{\mathcal{N}_{0,\psi}}\mathbf{\Lambda}_{\psi,1:Q}+\frac{\epsilon}{\mathcal{N}_{\psi,\pi}}\mathbf{I}_Q\right)^{-1}\mathbf{T}_{\psi,1:Q}^H\mathbf{\Gamma}_{0,\pi}\mathbf{T}_{\psi,1:Q}\left(\frac{1}{\mathcal{N}_{0,\psi}}\mathbf{\Lambda}_{\psi,1:Q}+\frac{\epsilon}{\mathcal{N}_{\psi,\pi}}\mathbf{I}_Q\right)^{-1}\mathbf{T}_{\psi,1:Q}^H\mathbf{d}(0)}\\ &= \mathbf{d}^H(0)\mathbf{T}_{\psi,1:Q}\left(\frac{1}{\mathcal{N}_{0,\psi}}\mathbf{\Lambda}_{\psi,1:Q}+\frac{\epsilon}{\mathcal{N}_{\psi,\pi}}\mathbf{I}_Q\right)^{-1}\mathbf{T}_{\psi,1:Q}^H\mathbf{d}(0),\end{aligned} \tag{A1}$$

$$\begin{aligned}\mathcal{F}_{\psi}(\mathbf{h}_{Q,2,\psi,\epsilon}) &= \frac{\mathbf{d}^H(0)\mathbf{T}_{\psi,1:Q}\left(\frac{1}{\mathcal{N}_{0,\psi}}\mathbf{\Lambda}_{\psi,1:Q}+\frac{\epsilon}{\mathcal{N}_{\psi,\pi}}\mathbf{I}_Q\right)^{-1}\mathbf{T}_{\psi,1:Q}^H\mathbf{\Gamma}_{0,\psi}\mathbf{T}_{\psi,1:Q}\left(\frac{1}{\mathcal{N}_{0,\psi}}\mathbf{\Lambda}_{\psi,1:Q}+\frac{\epsilon}{\mathcal{N}_{\psi,\pi}}\mathbf{I}_Q\right)^{-1}\mathbf{T}_{\psi,1:Q}^H\mathbf{d}(0)}{\mathbf{d}^H(0)\mathbf{T}_{\psi,1:Q}\left(\frac{1}{\mathcal{N}_{0,\psi}}\mathbf{\Lambda}_{\psi,1:Q}+\frac{\epsilon}{\mathcal{N}_{\psi,\pi}}\mathbf{I}_Q\right)^{-1}\mathbf{T}_{\psi,1:Q}^H\mathbf{\Gamma}_{\psi,\pi}\mathbf{T}_{\psi,1:Q}\left(\frac{1}{\mathcal{N}_{0,\psi}}\mathbf{\Lambda}_{\psi,1:Q}+\frac{\epsilon}{\mathcal{N}_{\psi,\pi}}\mathbf{I}_Q\right)^{-1}\mathbf{T}_{\psi,1:Q}^H\mathbf{d}(0)}\\ &= \frac{\mathbf{d}^H(0)\mathbf{T}_{\psi,1:Q}\left(\frac{1}{\mathcal{N}_{0,\psi}}\mathbf{\Lambda}_{\psi,1:Q}+\frac{\epsilon}{\mathcal{N}_{\psi,\pi}}\mathbf{I}_Q\right)^{-1}\mathbf{\Lambda}_{\psi,1:Q}\left(\frac{1}{\mathcal{N}_{0,\psi}}\mathbf{\Lambda}_{\psi,1:Q}+\frac{\epsilon}{\mathcal{N}_{\psi,\pi}}\mathbf{I}_Q\right)^{-1}\mathbf{T}_{\psi,1:Q}^H\mathbf{d}(0)}{\mathbf{d}^H(0)\mathbf{T}_{\psi,1:Q}\left(\frac{1}{\mathcal{N}_{0,\psi}}\mathbf{\Lambda}_{\psi,1:Q}+\frac{\epsilon}{\mathcal{N}_{\psi,\pi}}\mathbf{I}_Q\right)^{-1}\mathbf{I}_Q\left(\frac{1}{\mathcal{N}_{0,\psi}}\mathbf{\Lambda}_{\psi,1:Q}+\frac{\epsilon}{\mathcal{N}_{\psi,\pi}}\mathbf{I}_Q\right)^{-1}\mathbf{T}_{\psi,1:Q}^H\mathbf{d}(0)}.\end{aligned} \tag{A2}$$

Substituting Eq. (73) into Eq. (10), we obtain Eq. (A1) (where the parameter ω is removed for concision), which can be rewritten as

$$\mathcal{D}\left[\mathbf{h}_{Q,2,\psi,\epsilon}(\omega)\right] = \sum_{i=1}^{Q}\left[\frac{\lambda_{\psi,i}(\omega)}{\mathcal{N}_{0,\psi}}+\frac{\epsilon}{\mathcal{N}_{\psi,\pi}}\right]^{-1}|\mathbf{d}^H(\omega,0)\mathbf{t}_{\psi,i}(\omega)|^2. \tag{A3}$$

It is obvious that $\mathcal{D}[\mathbf{h}_{Q,2,\psi,\epsilon}(\omega)]$ is an increasing function of Q, and a decreasing function of ϵ. Substituting Eq. (73) into Eq. (56), we obtain Eq. (A2) (where the parameter ω is removed also for concision), which can be simplified as

$$\mathcal{F}_{\psi}\left[\mathbf{h}_{Q,2,\psi,\epsilon}(\omega)\right]=\frac{\sum_{i=1}^{Q}\frac{\lambda_{\psi,i}(\omega)}{\left[\frac{\lambda_{\psi,i}(\omega)}{\mathcal{N}_{0,\psi}}+\frac{\epsilon}{\mathcal{N}_{\psi,\pi}}\right]^2}\left|\mathbf{d}^H(\omega,0)\mathbf{t}_{\psi,i}(\omega)\right|^2}{\sum_{i=1}^{Q}\frac{1}{\left[\frac{\lambda_{\psi,i}(\omega)}{\mathcal{N}_{0,\psi}}+\frac{\epsilon}{\mathcal{N}_{\psi,\pi}}\right]^2}\left|\mathbf{d}^H(\omega,0)\mathbf{t}_{\psi,i}(\omega)\right|^2}. \tag{A4}$$

We can see that $\mathcal{F}_{\psi}[\mathbf{h}_{Q,2,\psi,\epsilon}(\omega)]$ is a decreasing function of the parameter Q. Differentiating Eq. (A4) with respect to ϵ, it can be found that $\mathcal{F}_{\psi}[\mathbf{h}_{Q,2,\psi,\epsilon}(\omega)]$ is an increasing function of the parameter ϵ, except for the case of $Q=1$.

Though it increases with the value of ϵ for $Q\geq 2$, the GFBR is always upper bounded by the maximum eigenvalue, $\lambda_{\psi,1}(\omega)$, of the matrix $\mathbf{\Gamma}_{\psi,\pi}^{-1}(\omega)\mathbf{\Gamma}_{0,\psi}(\omega)$, which can be verified by

$$\begin{aligned}\lim_{\epsilon\to\infty}\mathcal{F}_{\psi}\left[\mathbf{h}_{Q,2,\psi,\epsilon}(\omega)\right]&=\frac{\sum_{i=1}^{Q}\lambda_{\psi,i}(\omega)\left|\mathbf{d}^H(\omega,0)\mathbf{t}_{\psi,i}(\omega)\right|^2}{\sum_{i=1}^{Q}\left|\mathbf{d}^H(\omega,0)\mathbf{t}_{\psi,i}(\omega)\right|^2}\\&\leq\lambda_{\psi,1}(\omega).\end{aligned} \tag{A5}$$

Abhayapala, T. D., and Gupta, A. (**2010**). "Higher order differential-integral microphone arrays," J. Acoust. Soc. Am. **127**, 227–233.

Allen, J. B., and Berkley, D. A. (**1979**). "Image method for efficiently simulating small-room acoustics," J. Acoust. Soc. Am. **65**(4), 943–950.

Benesty, J., and Chen, J. (**2012**). *Study and Design of Differential Microphone Arrays* (Springer-Verlag, Berlin).

Benesty, J., Chen, J., and Cohen, I. (**2015**). *Design of Circular Differential Microphone Arrays* (Springer-Verlag, Switzerland).

Benesty, J., Chen, J., and Huang, Y. (**2008**). *Microphone Array Signal Processing* (Springer-Verlag, Berlin).

Benesty, J., Chen, J., Huang, Y., and Dmochowski, J. (**2007**). "On microphone-array beamforming from a MIMO acoustic signal processing perspective," IEEE Trans. Audio Speech Lang. Process. **15**(3), 1053–1065.

Benesty, J., Cohen, I., and Chen, J. (**2017**). *Fundamentals of Signal Enhancement and Array Signal Processing* (IEEE, Piscataway).

Benesty, J., Souden, M., and Huang, Y. A. (**2012**). "A perspective on differential microphone arrays in the context of noise reduction," IEEE Trans. Audio Speech Lang. Process. **20**(2), 699–704.

Brandstein, M., and Ward, D. B. (**2001**). *Microphone Arrays: Signal Processing Techniques and Applications* (Springer-Verlag, Berlin).

Buck, M. (**2002**). "Aspects of first-order differential microphone arrays in the presence of sensor imperfections," Eur. Trans. Telecomm. **13**, 115–122.

Buck, M., and Rößler, M. (**2001**). "First order differential microphone arrays for automotive applications," in *Proceedings of IWAENC*, Vol. 1.

Capon, J. (**1969**). "High resolution frequency-wavenumber spectrum analysis," Proc. IEEE **57**(8), 1408–1418.

Chen, J., Benesty, J., and Pan, C. (**2014**). "On the design and implementation of linear differential microphone arrays," J. Acoust. Soc. Am. **136**, 3097–3113.

Cox, H., Zeskind, R., and Owen, M. (**1987**). "Robust adaptive beamforming," IEEE Trans. Acoust. Speech Sign. Process. **35**(10), 1365–13764.

Cox, H., Zeskind, R. M., and Kooij, T. (**1986**). "Practical supergain," IEEE Trans. Acoust. Speech Sign. Process. **ASSP-34**(3), 393–398.

Derkx, R. M. M., and Janse, K. (**2009**). "Theoretical analysis of a first-order azimuth-steerable superdirective microphone array," IEEE Trans. Audio Speech Lang. Process. **17**(1), 150–162.

Doclo, S., and Moonen, M. (**2003**). "Design of broadband beamformers robust against gain and phase errors in the microphone array characteristics," IEEE Trans. Signal Process. **51**(10), 2511–2526.

Elko, G. W. (**2000**). "Superdirectional microphone arrays," in *Acoustic Signal Processing for Telecommunicationg*, edited by S. L. Gay and J. Benesty (Kluwer Academic, Boston), pp. 181–237.

Elko, G. W., Kubli, R. A., Morgan, D. R., and West, J. E. (**1996**). "Adjustable filter for differential microphones," U.S. patent 5,586,191.

Elko, G. W., and Meyer, J. (**2008**). "Microphone arrays," in *Springer Handbook of Speech Processing*, edited by J. Benesty, M. M. Sondhi, and Y. Huang (Springer-Verlag, Berlin), pp. 1021–1041.

Elko, G. W., and Meyer, J. (**2009**). "Second-order differential adaptive microphone array," in *Proceedings of the IEEE International Conference on Acoustics, Speech, and Signal Processing (ICASSP)*, pp. 73–76.

Elko, G. W., and Pong, A. T. N. (**1997**). "A steerable and variable first-order differential micropone array," in *Proceedings of IEEE ICASSP*, IEEE, Vol. 1, pp. 223–226.

Franklin, J. N. (**1968**). *Matrix Theory* (Prentice-Hall, Englewood Cliffs, NJ).

Frost, O. L. (**1972**). "An algorithm for linearly constrained adaptive array processing," Proc. IEEE **60**(8), 926–935.

Golub, G. H., and Loan, C. F. V. (**1996**). *Matrix Computations* (The Johns Hopkins University Press, Baltimore).

Huang, G., Benesty, J., and Chen, J. (**2017**). "On the design of frequency-invariant beampatterns with uniform circular microphone arrays," IEEE Trans. Audio Speech Lang. Process. **25**(5), 1140–1153.

Ihle, M. (**2003**). "Differential microphone arrays for spectral subtraction," in *Proceedings of IEEE Workshop Acoustic Echo Noise Control (IWAENC)*.

Kates, J. M. (**1993**). "Superdirective arrays for hearing aids," J. Acoust. Soc. Am. **94**(4), 1930–1933.

Kellermann, W. (**1991**). "A self-steering digital microphone array," in *Proceedings of the IEEE International Conference on Acoustics, Speech, and Signal Processing (ICASSP)*, pp. 3581–3584.

Kolundžija, M., Faller, C., and Vetterli, M. (**2011**). "Spatiotemporal gradient analysis of differential microphone arrays," J. Audio Eng. Soc. **59**(1/2), 20–28.

Koyama, S., Furuya, K., Wakayama, K., Shimauchi, S., and Saruwatari, H. (**2016**). "Analytical approach to transforming filter design for sound field recording and reproduction using circular arrays with a spherical baffle," J. Acoust. Soc. Am. **139**(3), 1024–1036.

Lehmanna, E. A., and Johansson, A. M. (**2008**). "Prediction of energy decay in room impulse responses simulated with an image-source model," J. Acoust. Soc. Am. **124**(1), 269–277.

Marshall, R. N., and Harry, W. R. (**1941**). "A new microphone providing uniform directivity over an extended frequency range," J. Acoust. Soc. Am. **12**, 481–497.

Olson, H. F. (**1946**). "Gradient microphones," J. Acoust. Soc. Am. **17**(3), 192–198.

Pan, C., Benesty, J., and Chen, J. (**2015a**). "Design of robust differential microphone arrays with orthogonal polynomials," J. Acoust. Soc. Am. **138**(2), 1079–1089.

Pan, C., Chen, J., and Benesty, J. (**2015b**). "Theoretical analysis of differential microphone array beamforming and an improved solution," IEEE Trans. Audio Speech Lang. Process. **23**, 2093–2105.

Park, M., and Rafaely, B. (**2005**). "Sound-field analysis by plane-wave decomposition using spherical microphone array," J. Acoust. Soc. Am. **118**(5), 3094–3103.

Schelkunoff, S. A. (**1943**). "A mathematical theory of linear arrays," Bell Syst. Tech. J. **22**(1), 80–107.
Schroeder, M. R. (**1965**). "New method for measuring reverberation time," J. Acoust. Soc. Am. **37**, 409–412.
Sena, E. D., Hacihabiboğlu, H., and Cvetković, Z. (**2011**). "A generalized design method for directivity patterns of spherical microphone arrays," in *Proceedings of the IEEE International Conference on Acoustics, Speech, and Signal Processing (ICASSP)*, pp. 125–128.
Sena, E. D., Hacihabiboğlu, H., and Cvetković, Z. (**2012**). "On the design and implementation of higher-order differential microphones," IEEE Trans. Audio Speech Lang. Process. **20**(1), 162–174.
Sessler, G. M., and West, J. E. (**1971**). "Directional transducers," IEEE Trans. Audio Electroacoustic **19**, 19–23.
Slavin, M. J. (**1987**). "Differential hearing aid with programmable frequency response," J. Acoust. Soc. Am. **81**(5), 1657.
Song, H., and Liu, J. (**2008**). "First-order differential microphone array for robust speech enhancement," in *Audio, Language and Image Processing, 2008. ICALIP 2008. International Conference*, pp. 1461–1466.
Teutsch, H., and Elko, G. W. (**2001**). "First- and second-order adaptive differential microphone arrays," in *Proceedings of IWAENC*, IEEE.
Torres, A. M., Cobos, M., Pueo, B., and Lopez, J. J. (**2012**). "Robust acoustic source localization based on modal beamforming and time–frequency processing using circular microphone arrays," J. Acoust. Soc. Am. **132**(3), 1511–1520.
Uzkov, A. I. (**1946**). "An approach to the problem of optimum directive antenna design," in *Comptes Rendus (Doklady) de l'Academie des Sciences de l'URSS*, pp. 35–38.
Wang, Y., Yang, Y., Ma, Y., and He, Z. (**2014**). "Robust high-order superdirectivity of circular sensor arrays," J. Acoust. Soc. Am. **136**(4), 1712–1724.
Warren, D. M., and Thompson, S. (**2006**). "Microphone array having a second order directional pattern," U.S. patent 7,065,220.
Weinberger, J., Olson, H. F., and Massa, F. (**1933**). "A uni-directional ribbon microphone," J. Acoust. Soc. Am. **5**(2), 139–147.
Yan, S., Sun, H., Svensson, U. P., Ma, X., and Hovem, J. M. (**2011**). "Optimal modal beamforming for spherical microphone arrays," IEEE Trans. Audio Speech Lang. Process. **19**(2), 361–371.
Zhao, L., Benesty, J., and Chen, J. (**2014**). "Design of robust differential microphone arrays," IEEE Trans. Audio Speech Lang. Process. **22**(10), 1455–1466.
Zheng, Y. R., Goubran, R. A., and El-Tanany, M. (**2004**). "Experimental evaluation of a nested microphone array with adaptive noise cancellers," EEE Trans. Instrum. Meas. **53**(3), 777–786.